2022-12-01

Using Ground Penetrating Radar to Investigate Controls on Pedogenic Calcium Carbonate Distribution in Dryland Critical Zones

Nohemi Valenzuela Garay
University of Texas at El Paso

USING GROUND PENETRATING RADAR TO INVESTIGATE CONTROLS ON PEDOGENIC CALCIUM CARBONATE DISTRIBUTION IN DRYLAND CRITICAL ZONES

NOHEMI VALENZUELA GARAY

Master's Program in Geological Sciences

APPROVED:

Mark Engle, Ph.D., Chair

Lin Ma, Ph.D.

Elizabeth La Rue, Ph.D.

Stephen L. Crites, Jr., Ph.D.
Dean of the Graduate School

USING GROUND PENETRATING RADAR TO INVESTIGATE CONTROLS ON PEDOGENIC CALCIUM CARBONATE DISTRIBUTION IN DRYLAND CRITICAL ZONES

by

NOHEMI VALENZUELA GARAY

THESIS

Presented to the Faculty of the Graduate School of

The University of Texas at El Paso

in Partial Fulfillment

of the Requirements

for the Degree of

MASTER OF SCIENCE

Department of Earth, Environmental, and Resource Sciences

THE UNIVERSITY OF TEXAS AT EL PASO

December 2022

Acknowledgements

The material is based upon work supported by the national science foundation NSF award #2012475. A big thank you to Dr. Diane Doser, Galen Kaip, Dr. Lixin Jin, Christian Leach, Valeria Molina, Elizabeth Gardea, Kamal Nyaupane, and the GEOSENSE Team.

Abstract

Caliche or pedogenic calcium carbonate ($CaCO_3$) layers are a common feature of arid soils, but the environmental controls on their distribution are not fully understood. Caliche layers are thought to play an important role in shallow subsurface water storage and movement, due to their water retention capacity and ability to impede vertical water transport (Hennessy et al., 1983). Therefore, caliche distribution and stability play a role in controlling water distribution in arid lands. However, due to its largely subsurface nature, caliche can be difficult to investigate and map without significant effort. I hypothesize that noninvasive geophysical methods, such as ground-penetrating radar (GPR), may be an ideal approach to characterize shallow caliche layers as means to understand controls on its distribution.

The goals of this research are to: 1) apply GPR to document the distribution and nature of subsurface caliche layers; 2) investigate the physical and chemical stability of caliche relative to its distribution at specific dryland sites; 3) examine the role of caliche layers in regulating soil water storage and movement. This research was conducted at two sites (one piedmont and one playa site) in the Chihuahuan desert at Jornada Experimental Range (JER) near Las Cruces, New Mexico. Seasonal GPR data have been collected to determine ideal conditions (e.g., soil moisture content) to map caliche with GPR in dryland environments. Water movement through and soil erosion above caliche layers were used as indicators of its physical and chemical stability, respectively, to understand caliche's chemical and physical stability across the two sites. Vertical water fluxes and soil moisture content in the shallow vadose zone were investigated using time series data from vertical profiles of Time Domain Reflectometry (TDR) soil moisture probes at multiple locations in the study sites. Surface stability was assessed through the implementation of the Revised Universal Soil Loss Equation (RUSLE), which has been largely used in soil

science to determine soil erodibility (Benavidez et al., 2018; Chandramohan et al., 2002). GPR radargrams successfully identified the top surface of the shallowest caliche layer; those depths correlate with hand augering observations. Reflectors in GPR radargrams that are roughly coincident with the bottom of the caliche layer were also observed in several of the soil profiles. On the piedmont site, caliche was both physically and chemically stable on the Jornada I surface (JI), while it is physically but non chemically stable on the Organ surface (Qo). This research has demonstrated the utility of GPR to investigate the spatial distribution of caliche layers, and their presence relative to indicators of physical surface stability and chemical caliche stability. It also points toward the processes that lead to caliche formation or erosion in dryland environments.

Table of Contents

List of Tables

Table of Figures

Section 1: Introduction

Caliche, or pedogenic calcium carbonate layers, are a common feature of arid and semi-arid soils. Caliche layers typically form in the near subsurface (depths <2 m) where low soil P_{CO2} and high evapotranspiration rates favor $CaCO_3$ formation (Zamanian et al., 2016). In dryland vadose zones, plant water availability is impacted by the presence of caliche layers, resulting from their water-retaining properties (Hennessy et al., 1983) and by acting as a barrier to roots and vertical water flow movement (Duniway et al., 2007). At the Jornada Experimental Range (JER) near Las Cruces, New Mexico, diffuse recharge across the basin is generally thought to be minimal (except perhaps in playas and active channels; McKenna and Sala, 2018; Schreiner-McGraw et al., 2020), and the water table is too deep to support plant growth (Havstad et al., 2006). Where present, caliche layers may contribute to low recharge by impeding infiltration (Havstad et al., 2006; Duniway et al., 2007, 2010). Low infiltration rates impact vegetation patterns, topography, and ecosystem stability. Given the relatively strong control that caliche has on shallow soil water distribution and movement, understanding its distribution and controls thereof are critical. This study investigates the distribution of caliche layers at an upland piedmont site at JER and evaluates their physical and chemical stability through hydrogeophysical approaches.

Caliche layers of the Chihuahuan desert of the southwestern U.S. and northern Mexico are well documented and have been heavily investigated, but there is a lack of understanding their controls, and extent of distribution (Duniway et al., 2007, 2010; Havstad et al., 2006; Hennessy et al., 1983; Gile et al., 1979; Monger, 2006). For example, caliche water retaining properties and corresponding retention curves were previously developed (Hennessy et al., 1983; Duniway et al., 2007). This research focuses on study sites within the JER, in the far northern

extent of the Chihuahua desert, as part of a large-scale research investigation of dryland Critical Zones (Figure 1). Despite these efforts, the extent and distribution of caliche layers within the

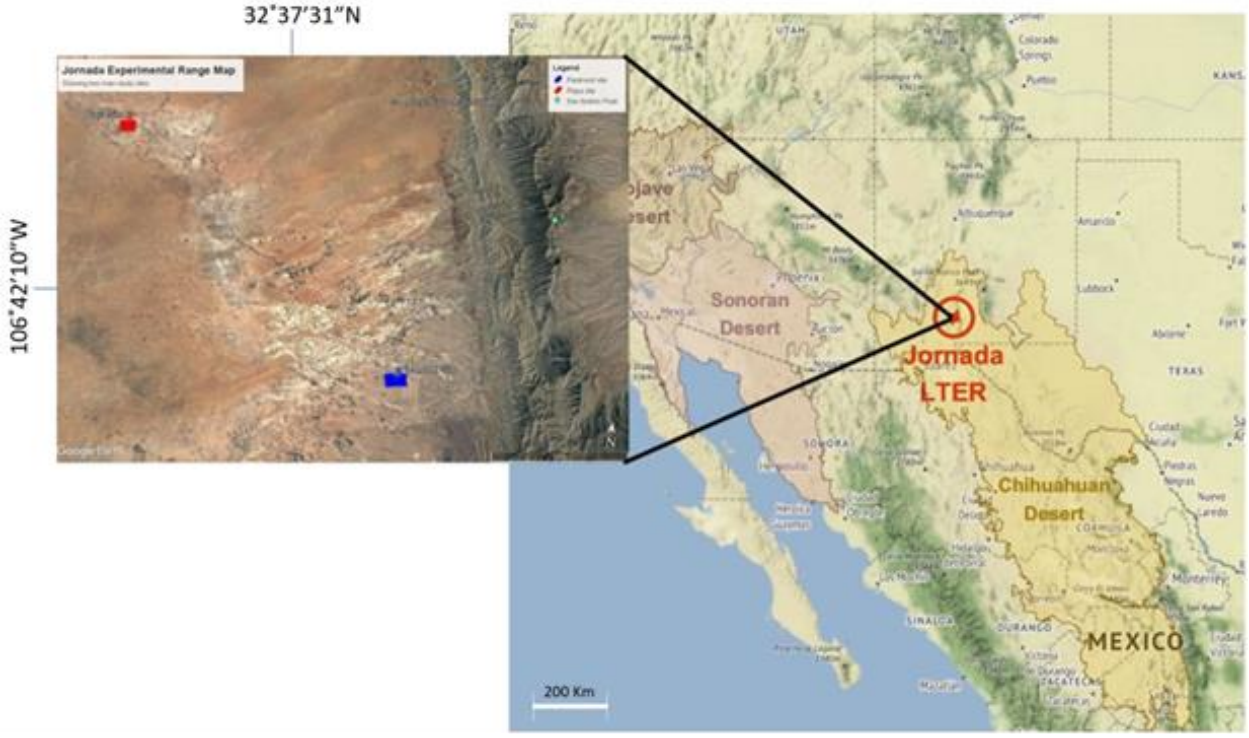

Figure 1: Jornada Long-Term Experimental Range location shown in a red star along with major deserts in western US, zoom in photo of our study sites. Credit: Jornada Basin LTER Website: Jornada map (fp-slider1)-Jornada Basin LTER (nmsu.edu).

JER are not well known; a generalized map of caliche stages at JER is available but does not provide detailed information on caliche distribution or stage (USDA Spatial Data Laboratory, 2003). Two reasons for this lack of insight regarding caliche distribution are its subsurface nature and a lack of surface features or manifestations. Ground-penetrating radar (GPR), a geophysical method that examines variations in shallow subsurface electrical properties in the form of radio wave reflections, has been successful at mapping shallow subsurface layers across a broad range of natural sites (Zajicova and Chuman, 2019; Neal et al., 2004; Young and Sun, 1999; Takahashi et al., 2015; Zhang et al., 2014). However, potentially problematic electrical properties of certain subsurface media, including salt- and clay-rich layers that exhibit high electrical conductance

(Wilson et al., 2005), make the ability of GPR methods to accurately map the caliche layers in dryland environments relatively untested. Moreover, previous work conducted in wetter environments found significant differences in the ability of GPR methods to resolve key subsurface structures depending on seasonal variations (Zhang et al., 2014). Minimal information is available about seasonal resolution improvements using GPR in arid environments. This research provides a framework to map caliche layer boundaries and analyze its stability and controls on their distribution across drylands utilizing GPR and hydrological methods.

Caliche layers exhibit a lagged response to climatic shifts. At JER they formed during the colder, wetter Pleistocene Epoch, hence they are likely not in equilibrium with current climate conditions (Monger, 2006; Gile, 1999). From 1957 to 1972, a group of about 100 geologists and soil scientists participated in the Desert Soil-Geomorphology Project; their study site was part of the Chihuahuan desert located in Southwest New Mexico (Gile et al., 1979). The Desert Project's goals were to find relations between morphology, genesis, and distribution of desert soils and landscape (Gile et al., 1979). Associated research also contributed to the mapping and understanding of mapping soils in arid regions (Gile et al., 1979). Findings included the discovery that calcium sources arrive due to the atmospheric inputs like dust and rain, instead of sources being remnants or an ancient water table (Monger et al., 2009). The calcium sources are carried vertically into the subsurface by infiltrating precipitation and concentrated through subsurface evaporation, leading to the formation of well-developed caliche layers (Canup, 2000). Because scientists have predicted that climate change will prolong the warm season and reduce precipitation in the southwestern United States (Archer and Predick, 2008), caliche stability is likely to increase where it is already present but may be less likely to form due to the decreased

precipitation. It is important to understand the controls on caliche stability and its distribution due to their lagged response to changes in the environment. We hypothesize that indurated caliche layers (Stage IV; described below) will only be present where it is both physically and chemically stable for long periods. These conditions are thought to exist below elevated surfaces covered by desert pavement, where water flux and rates of erosion/deposition are low. Study sites have been chosen to reflect variation in likely caliche stability (Figure 2).

Figure 2: Matrix visualizing study sites and their physical and chemical caliche stability based on initial hypotheses.

I assessed physical and chemical stability at sites with and without caliche, to identify possible controls on caliche distribution and stability. Quantifying vertical water flux and soil moisture content in soil profiles provides insight into chemical stability, as high-water fluxes and prolonged high-water content prevent the buildup of ionic precursors of shallow caliche layers by keeping calcite solubility below its saturation index (Monger, 2006; Zamaian et al., 2016).

Precipitation is a major variable in controlling caliche distribution in the soil profile; annual precipitation below 500 mm has a higher probability of producing shallow caliche layers (<75 cm depth). Higher annual precipitation (>500 mm) decreases the probability of caliche forming (Zamanian et al., 2016). Physical stability (e.g., the relative rate of erosion or deposition) will be partially examined through the application of the Revised Universal Soil Loss Equation (RUSLE) to assess the relative erosivity of various surfaces. RUSLE was created to predict annual soil loss due to runoff for agricultural purposes, but it has been adapted for natural conditions (Wischmeier and Smith, 1978; Chandramohan and Durbude, 2002). By examining the chemical and physical stability of caliche at study sites with and without caliche, an insight into the controls on caliche heterogeneity will be produced and the work will assess if GPR is a valid method to study these layers in arid regions.

Section 2: Background

2.1 Geological Background

The JER was established by the U.S. Department of Agriculture in 1912 to study the effects of grazing on arid lands (Rango et al., 2003). In 1998, the site became a member of the Long-Term Ecological Research (LTER) program for the National Science Foundation (Figure 1). Throughout its history as a research site, soil, hydrology, and biological features at JER have been investigated (Havstad et al., 2006; Hennessy et al., 2006; Duniway et al., 2007, 2010; Rango et al., 2003). The JER is located within the Jornada del Muerto geological basin and is part of the Rio Grande rift system, which is controlled by a north-south trending fault that has been active since the Oligocene epoch (Havstad et al., 2006). The site is influenced by three bounding mountain ranges and the ancestral Rio Grande River. The San Andres Mountains, consisting mostly of limestones and carbonates, bound the eastern edge of JER; the basalt-dominated Doña Ana Mountains are found in the southwest corner of JER; and the Organ Mountains, composed of granite, ignimbrites, and tuff are located on the southeast border of the site. The ancestral Rio Grande is thought to have passed through the Jornada del Muerto Basin about 1.6 million years ago, and the river played an important role in shaping the basin stratigraphy (Mack et al. 1996). Geomorphology of the site is characterized by westward dipping piedmont slopes, alluvial fan remnants, and playas adjacent to the San Andres Mountains, which transition westward to lower elevations and several playas. Soils are primarily calcareous, with some sites having developed indurated caliche horizons, and little to no organic content (Havstad et al., 2006).

All six stages of the continuum of caliche development are present at JER. The earliest form of caliche begins as small fragments of carbonate begin to accumulate in shallow soil, these

often occur as fine strings or coatings on rocks (Stage I). After some time, these fragments may begin to form larger coatings and eventually carbonate nodules (Stage II). Enough carbonate may accumulate to form a cemented Bk horizon (Stage III) and may even form laminae on top (Stage IV). During its final stages, it is a completely cemented horizon with possible secondary porosity (Stage V and VI) (Chakraborty et al., 2017). Studies that investigated hydrologic properties of caliche at JER found that often the bulk density of caliche is greater than the bulk density of the soils, caliche has water-retaining properties, and possible lateral flow may occur above caliche layers (Hennessy et al., 1983).

The JER has been utilized for decades to understand the relationships between soil, water, and vegetation with time. Buffington and Herbel (1965) examined vegetation populations and found that the proportion of the site dominated by grasslands decreased from 90% to < 25% between 1858 and 1963. They identified mesquite and creosote as the dominant vegetation type by the end of their study period and concluded this plant species shift was the result of grazing and the slow drought recovery by some grass species (Buffington and Herbel, 1965). Shifts in vegetation are important in controlling water and soil stability because plants have root systems of varying behavior (Gibbens and Beck, 1988). One infiltration study showed dense vegetation cover is more resistant to erosion and runoff at JER than unvegetated sites. (Tromble, 1980). Similarly, Li et al. (2007) revealed that wind erosion increases when lateral plant cover falls below 9%. Other studies have examined connections between widespread caliche layers on soil moisture and plant-available water. Duniway et al. (2010) suggested that the roots of certain plants may be able to access the water held by caliche. This research also found that caliche-cemented horizons exhibit higher volumetric water content than those containing no cemented horizons (Duniway et al., 2010). Recharge through deep vadose zones found at dryland sites,

such as JER is generally not through diffuse recharge of the water table. Recent studies at JER suggest that there may be recharge beneath active channels and/or playas (Reuter et al., 2021) as well as mountain front recharge.

2.2 Study Sites Background

This research focuses on two main study sites within JER: the piedmont and playa sites (Figure 1). The piedmont study site is located about 10 km west of the San Andres Mountains. Geomorphologically, the site is characterized by: 1) higher elevation surfaces (Jornada I surface of Gile, 1999; herein referred to as JI) where creosote (*Larrea tridentata*) and mesquite (*Prosopis glandulosa*) are the dominant vegetation and soil consists of a moderately developed desert pavement overlying a loamy soil; and 2) younger, lower elevation surfaces (Organ surface of Gile, 1999; herein referred to as Qo) adjacent to ephemeral channels where black grama grasses (*Bouteloua eriopoda*) are the dominant vegetation and soils are generally finer (clay loam). Figure 3 summarizes textural class analysis for soils below the two surfaces. These two geomorphic surfaces at the piedmont site are of interest due to their variable properties and

differences in caliche distribution. Linear transects, along which field measurements are focused, were established to cross each surface one or more times (Figure 4).

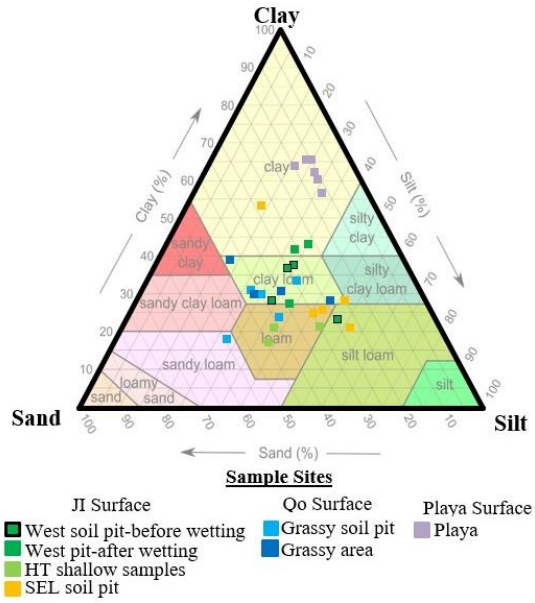

Figure 3: Textural class analysis summary of samples collected along transects a Jornada Experimental Range.

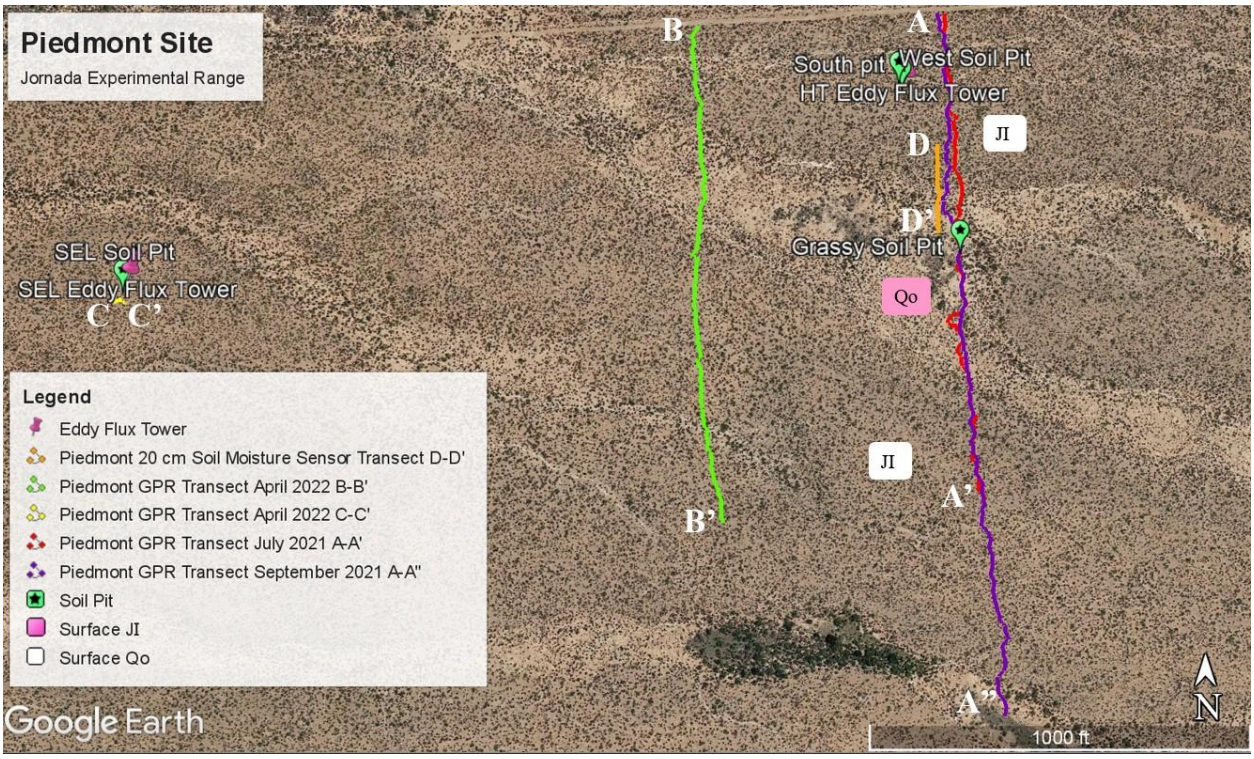

Figure 4: Piedmont study site map showing GPR transects, soil pit arrays/transects, and Eddy Flux tower locations.

The playa study site is located about 25 km northwest of the piedmont study site and can be classified into three zones based on differences in vegetation densities and type, and topography (Figure 5). Playas form in topographical lows, sometimes in arid environments, where water accumulates after large and/or multiple small rainfall events. Since playas are sites of high downward subsurface water flux, caliche is not generally observed below them. Playas provide important sources of nutrients to the ecosystems surrounding them and maybe sites of recharge. The soils at the Red Lake Playa site are very clay-rich (69%), containing a high concentration of gypsum and smectite swelling clays, which have high water content (Monger, 2006). Transects of investigations at this site were established to cover these four surfaces of interest with different vegetation densities shown in Figure 5.

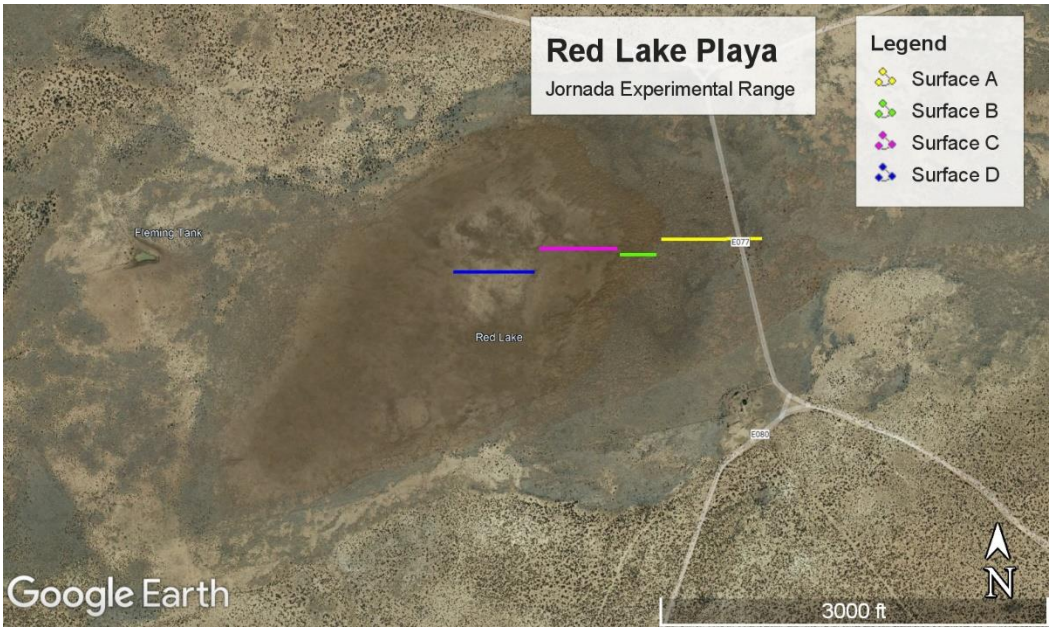

Figure 5: Different surfaces at playa location classified by differences in vegetation density and slope.

Section 3: Methods

3.1 Geophysical Methods

Ground-penetrating radar (GPR) is useful for imaging boundaries separating layers of contrasting electrical properties (i.e., dielectric permittivity) in the shallow subsurface (generally depths <5 m) and produces minimal disturbance, which can be advantageous over destructive sampling methods. The GPR method is often used to locate buried human infrastructure (e.g., tanks and pipelines) but has also proven useful in identifying layers, caves, moisture, and other natural subsurface structures in soil studies (Young and Sun, 1999; Zhang et al., 2014; Takahashi et al., 2015). Electromagnetic signals are transmitted into the subsurface and a receiver identifies reflections back to the surface, which occur when radar waves cross boundaries of contrasting materials (Zajicova and Chuman, 2019). The strength of these reflections can be quantified by the reflection coefficient (r), which is a function of the relative difference in the dielectric permittivity of the contrasting materials at a layer boundary (Eq. 1):

$$r = \frac{\sqrt{\varepsilon_U} - \sqrt{\varepsilon_L}}{\sqrt{\varepsilon_U} + \sqrt{\varepsilon_L}}, \text{ Eq. 1}$$

where ε_U is the dielectric permittivity of the upper layer and ε_L is the dielectric permittivity of the lower layer. Dielectric permittivity is a measure of the amount of energy stored during polarization (Neal, 2004). From Eq. 1, the larger the relative differences in the dielectric permittivity between soil boundaries, the higher the GPR reflection. The depth of a strong reflector (d) can be calculated for low salinity and low clay content soils (Zhang et al., 2014):

$$d = \frac{vt}{2}, \text{ Eq. 2}$$

where t is the two-way travel time and

$$v = \frac{c}{\sqrt{\varepsilon}}, \text{ Eq. 3}$$

where c is the speed of light (0.3 m/ns) and ε is dielectric permittivity. If the wave velocity is accurately known, GPR can both identify boundaries or fronts where electrical properties of materials vary greatly across a boundary and the depth of the corresponding boundary. These geophysical relationships have allowed for GPR to distinguish layering in sediments, distribution and movement of soil water, and, in some cases, plant roots.

GPR data were collected using a 250 MHz Noggin SmartCart® GPR (Sensors & Software Inc.) coupled to a Real-Time Kinematic (RTK) Global Positioning System (GPS) that uses a Topcon GB-1000 receiver. Global Positioning System (GPS) allowed for acquisition of precise measurement locations. GPR acquisition used a transmitter and receiver signal that collected data in eight stacks, every 0.25 m. Raw GRP data were processed using EKKO (version 5) software. Linear GPR transects were established in both study sites (as described above) to identify subsurface structures, potentially including the caliche-soil interface and wetting front related to vertical water movement and distribution. Repeated GPR measurements along transects collected during wet vs. dry soil moisture conditions helped validate the location of the subsurface caliche layers (e.g., caliche-soil) and document changes or influence of resolution due to soil moisture variability and other seasonal changes.

GPR measurements at the Piedmont study site were focused along three north-south transects, A-A'/A" and B-B' and a smaller west-east transect C-C' (Figure 4). These transects were selected to cross the higher elevation, creosote-dominated surfaces (JI surface), and lower elevation, grass-dominated surfaces (Qo surface). The A-A'/A" and B-B' transects cross a site where two arroyos conflux, on the Qo surface, making it ideal to study caliche distribution relative to variations in topography (Table 1 details the transects). At the piedmont study site, the first GPR measurements (known as 21-PW) were collected along the 450 m long transect A-A'

(and in the reverse direction: A'-A) on July 10, 2021, after a period of intense monsoonal rainfall (referred to as the wet condition) shown in Figure 4. Another, longer set of GPR measurements (21-PD; 650 m) were collected along the A-A" transect in both directions near the end of summer (September 12, 2021), when soil moisture conditions were much drier (Figure 4). As part of this research, an additional GPR transect B-B' was collected 200 m downhill (west) from the original transect (A-A'/A") to capture a larger extent of the piedmont slope (Figure 4). In addition, transect C-C' has been established along a soil pit installed near SEL eddy flux tower on the west side of the piedmont site, intended to cross the bottom of the caliche found during sensor installation. GPR measurements were collected during drier periods (September 2021 and April 2022) and the wetter monsoon season (July 2021), allowing for a contrast in GPR responses to variations in soil moisture and distribution. C-C' GPR transect was collected next to the soil moisture senor pit near the SEL Eddy flux tower, where the bottom of uppermost caliche layer was identified in a soil pit. Measurements along these additional transects are intended to aid in the investigation of caliche heterogeneity, and stability along the piedmont slope.

Table 1: Transect and GPR collection details.

Table 1: GPR Collection Events			
GPR collection	Transect surveyed	Date Collected	Length
21-PW	A-A'	July 10, 2021	450 m
21-PL	E-E'	August 4, 2021	600 m
21-PD	A-A"	September 12, 2021	600 m
22-PD	B-B'	April 15, 2022	400 m

22-PT	C-C’		6 m

The GPR approach was also utilized at the Playa site. The JER playas are known not to contain caliche horizons, since they are thought to flush water and salts below the near-surface and are sites of net sediment deposition, rather than erosion (Havstad et al., 2006) potentially leading to too much sedimentation to allow for caliche to form at a consistent depth. Playas at JER have been documented to have a high clay content and maybe possible recharge hotspots (Havstad et al., 2006). High clay content generates GPR signal attenuation, often producing poor GPR response (Zajicova and Chuman, 2019). GPR data (21-PL) were collected along transect E-E’ at the playa site on August 4, 2021, to confirm there is no caliche layer or other unexpected layers.

3.1.1 Ground Penetrating Radar Processing

EKKO Version 5 was used to process GPR radargrams after data collection. Background subtraction and dewow filters were applied to the radargrams; these filters aid in the visualization of the data by removing low-frequency components and background noise. AASEC2 (Spreading and Exponentially Calibrated Compensation) gain was applied to the radargrams, which incorporates linear and exponential time gain functions. Velocity calibrations during each GPR measurement event were determined using Equation 3 and permittivity data from TDR sensors from the west pit from depths of 20 and 32 cm. EKKO V.5 also has a slice view feature that allowed viewing the strength of reflections on slices of the radargram every 10 cm along each transect measurement.

3.2 Auger Transacts

Along the A-A” transect (Table 1 and Figure 4), hand augering was performed at 25 m intervals to determine the estimated minimum depth of caliche. Hand augering has also been

performed along the B-B' transect at 50 m intervals (the green transects in Figure 4). Total depth or depth to refusal and observations of soil properties (e.g., texture, caliche content) were recorded. The corresponding data aided in verifying the top of the caliche layer relative to GPR interpretations and to calibrate velocity measurements. Soil samples were collected to determine soil textures above the caliche layer (Figure 3).

3.3 Physical Stability

Given that I hypothesized that caliche can only form or exist for long periods in sites that are both physically stable (i.e., limited erosion or deposition) and chemically stable (i.e., low vertical water flux and/or high perennial soil moisture content), this section focuses on approaches to investigate the former for specific surfaces are the piedmont and playa study sites.

3.3.1 Revised Universal Soil Loss Equation

Potential soil erosion at each site was estimated using the empirical Revised Universal Soil Loss Equation (RUSLE). The RUSLE is the most widely used method to quantify soil loss due to erosion by water (Wischmeier and Smith, 1978; Renard and Freimund, 1993). Factors included in the RUSLE equation include rainfall-runoff erosivity (R), soil erodibility (K), slope length (L), slope steepness (S), cover and crop management (C), and support practice (P):

$A = R * K * L * S * C * P$. Eq. 4

For natural sites, such as in this study, a factor of 1 is applied to the crop management and support practice terms, removing their effect from the calculation (Benavidez et al., 2018; Chandramohan and Durbude, 2002). Each term in the equation must be calculated independently, as described below.

3.3.1.2 Rainfall erosivity (R)

The R factor represents erosion caused by rainfall and the associated runoff. It is a function of the average erosion index (EI_{30}) in a year, where E is storm kinetic energy and I_{30} is the maximum 30 min intensity (Wischmeier and Smith, 1978). Equations 5 and 6, proposed by Renard and Freimund (1993), were utilized to determine R:

$$R = 587.8 - 1.219P + 0.004105P^2 \; when \; Precipitation(P) > 850 \frac{mm}{yr}, \qquad \text{Eq. 5a}$$

$$R = 0.0483 * P^{1.610} \; when \; Precipitation \; (P) < 850 \frac{mm}{yr}, \qquad \text{Eq. 5b}$$

and

$$Fournier \; Index(F) = \frac{\sum_{i=1}^{12} P_i^2}{\sum_{i=1}^{12} P}, \qquad \text{Eq. 6a}$$

where P_i is the monthly precipitation, P is annual precipitation, and

$$R = 0.07397F^{1.847} \text{ when } F < 55 \text{ mm}, \qquad \text{Eq. 6b}$$

and

$$R = 95.77 - 6.081F + 0.4770F^2 \text{ when } F \geq 55 \text{ mm}, \qquad \text{Eq. 6c}$$

Each set of equations (5 vs. 6) provides different results since they are empirical regression equations generated from mean annual precipitation and the Fournier index; a comparison of the corresponding results provides a range of variability for this term in RUSLE. R is calculated using metric units (MJ mm ha^{-1} h^{-1} yr^{-1}), then converted to SI units (hundreds of foot tons inch $acre^{-1}$ h^{-1} yr^{-1} by dividing by 17.02 (Foster et al., 1981). Monthly and annual precipitation data was collected from eddy flux towers installed at the piedmont study site (Tweedie et al., 2021).

3.3.1.3 Soil erodibility (K)

This factor accounts for potential erosion as a function of soil physical properties. K is a quantitative measurement of the soil loss normalized to a specified unit plot (72.6 ft long with a uniform 9% slope), continuously fallow, and tilled up and downslope (Wischmeier and Smith 1978; Renard and Freimund 1993). K was calculated using the method of Wischmeier and Smith (1978), which is valid for soils with less than 70 % silt content (Eq. 7):

$$K = \frac{\left(2.1M^{1.14}(10^{-4})(12-a)\right)+(3.25(b-2))+(2.5(c-3))}{100}, \qquad \text{Eq. 7}$$

where *M* is the particle size parameter (silt%(100-clay%)), *a* is the percent soil organic matter, *b* is a soil structure code used in soil classification (1 = very fine granular; 2= fine granular; 3= medium or coarse granular; and 4=blocky, platy, or massive) and *c* is the soil profile permeability class (1 = rapid, 2 = moderate to rapid; 3 = moderate; 4 = slow to moderate; 5 = slow; 6 = very slow).

This approach utilizes soil textural class data, which has been determined by analyzing samples collected from various locations and depths in both study sites. Textural analysis was completed using hand sieving for sand-size particles and quantifying the rest of the fraction using a METER Pario, which utilizes the Integral Suspension Pressure method (ISP/ISP+) for the silt and clay fraction (Durner et al., 2017; Durner and Iden, 2021). Organic matter data content was taken from literature, and other researchers working in the project site.

3.3.1.4 Slope length (L) and Slope steepness (S)

These two factors represent possible soil erosion by water, resulting from slope geometry. The combined LS term is the ratio of soil loss from a slope at a given site relative to soil loss from a unit plot (slope with a length of 72.6 ft and steepness of 9%: Wischmeier and Smith,

1978). Many authors merge these two factors into a single input for field studies where LS is determined from slope length and slope angle:

$$LS = \left(\frac{\lambda}{72.6}\right)^{m} (65.41 * \sin^2(\theta) + 4.56 * \sin(\theta) + 0.065), \qquad \text{Eq. 8}$$

where λ = slope length, θ = slope angle, and the m factor depends on slope (>5% = 0.5; 3.5% to 4.5% = 0.4; 1% to 3% = 0.3, and <1% = 0.2).

Slope measurements were calculated at multiple surfaces which intersect the GPR transects using a DEM created from LiDAR data. This factor can have the largest errors due to assumptions made in calculations that may not account for all changes in topography (Benavidez et al., 2018), so results from the various methods will be compared.

3.4 Chemical Stability

Chemical caliche stability used water flux and perennial soil moisture content as a proxy for dissolution or caliche precursor transport away from sites of potential caliche formation, and possible precipitation of caliche at the specified sites. Since it is known that caliche is formed by precipitation and evaporation of shallow soil moisture, identifying the water flux patterns and soil moisture can identify sites where caliche may form (Zamanian et al., 2016).

3.4.1 Soil Moisture Distribution and Movement

Soil water content data can be used to provide information on perennial soil moisture content and whether or not water infiltrates through the soil profile or is captured by a caliche layer. In sites where caliche is present, thicker caliche layers may develop if there is shallow evaporation and precipitation since the calcium arrives from atmospheric inputs. In sites where caliche is absent, shallow evaporation of infiltrating precipitation may cause caliche to slowly start forming following rapid ET. Caliche formation requires cycles of evaporation and re-precipitation of calcium parent material at depth. The amount of precipitation plays a role in

determining the depth of caliche formation (Zamanian et al., 2016). Therefore, water movement through soils gives insight to whether caliche may form, continue to develop ticker layers, or may not form. In this study, vertical profiles of TDR probes were installed at five sites (four at the Piedmont study site, and one at the Playa study site), and along one transect (D-D' going from JI to Qo surface) to determine the depth of the water infiltration, and movement in response to precipitation events and therefore caliche chemical stability, since water flux largely controls chemical reactions that support caliche formation/dissolution (Zamanian et al., 2016). The TDR probes were installed at depths above the caliche, within the caliche (at one site), and below the caliche (at one site). The probes above the caliche were installed at depths of 5-10 cm, 10-20 cm, and 30-50 cm below ground surface depending on where the top of the caliche is found, if any. The D-D' TDR transect, perpendicular to slope from the JI surface to the Qo surface, includes TDR probes at a 20 cm depth along points A-F (Figure 4). At the piedmont site, probes have been locally calibrated using a regime developed by Dr. Lin Ma. A full list of depths and locations of current TDR profiles can be seen in Table 2, and a map showing their locations can be seen in Figure 4.

Table 2: Soil pit sensor locations, depths, and observations.

Table 2	
West Soil Pit, Piedmont Study Site Location: 32'35'0."2"N, 106°37'41.32"W	
Depth of soil moisture probe (cm)	Notes
11	67.0 cm to the bottom of the soil pit, 37.5 cm top of caliche, there are roots inside the caliche extend to the
20	
32	

50 (w/in caliche)	bottom of the pit, above caliche density of roots is larger, some shallow rocks exhibit caliche coating.
South Soil Pit, Piedmont Study Site Location: 32’35'0.”2"N, 106°37'41.20"W	
Depth of soil moisture probe (cm)	Notes
10	No probes installed inside caliche; the soil has higher gravel content
20	
29	
SEL Soil Pit, Piedmont Study Site Location: ’2”34'55"N, 106°38'6"W	
Depth of soil moisture probe (cm)	Notes
11	0-33 cm gravel-rich fine soil, 33 cm to top of the caliche layer, indurated layer, and large gravels at the top of the caliche layer 33-80 cm, 80 cm below fine caliche, matrix-supported gravel.
17	
25	
40	
100.5 (below caliche)	
Playa Soil Pit, Playa Study Site Location: 32°’2'44.”7"N, 106°49'49.22"W	
Depth of soil moisture probe (cm)	Notes
10	No caliche layer at this site
20	
30	

50	
90	

Section 4: Results

4.1 Augering

Based on observations from hand augering and soil pits at our study sites, the depth to the upper surface of the shallowest caliche layer was estimated to range from ~21-46 cm, where present. Refusal depth measurements generated from augering coincide with the interpreted top caliche boundary from GPR data as seen in Figures 6-9. In all auger holes below the JI surface, apparent large caliche nodules were intercepted, which impeded progress. In some cases, fine caliche dust, caliche covered nodules, and caliche nodules were also often observed at depths just above the depth of refusal. Below the Qo surface, caliche dust and small nodules were seen at deeper depths (0.8-1.6 m deep) than for the JI surface. Hand augering depths measured along A-A' and B-B' agree well with each other.

4.2 Ground Penetrating Radar Measurements

The GPR data were collected throughout wetter to drier conditions (i.e., July 2021, September 2021, and April 2022 respectively), suggest that depth to the top of the shallowest caliche layer boundary ranges from ~20-50 cm (where present) while the bottom layer for the same caliche are ~ 1 m deep (Figures 6-9). Given the high dielectric permittivity of water (~80) relative to unsaturated sand (2.55-7.5), silt, or clay (2.5-5), wet soil moisture conditions were expected to improve the caliche layer imaging since differences in electrical properties between low water-caliche and wetter porous soil above the caliche will be larger due to saturated soil (Neal, 2004). In 2021, JER received more rainfall (250 mm) than usual (200 mm), due to an abnormally active monsoon season. The 21-PW radargram, collected during the wetter period along A-A', has stronger air-ground reflectors at the top of the JI surface than was observed when compared to the same reflector in the 21-PD radargram, which was collected during drier

conditions (Sept. 2021). Exposed caliche in channels also produce stronger reflections at the surface than air-ground interfaces outside of the channels and can be seen in 21-PW, 21-PD, and 22-PD radargrams. Caliche is consistently seen below JI surfaces (depths of 0.3-0.5 m) but was not identified at similar depths below Qo surfaces. A small reflector beneath the Qo surface in the radargram from 21-PD was observed, however. The identified top of the caliche extends approximately further 50 m south on the 21-PW radargram than on the 21-PD radargram (both largely along the same transect), suggesting that this surface was in some cases more easily mapped during wetter soil moisture conditions. There are no other prominent differences identified between the 21-PW and 21-PD radargrams. A deeper reflector was also observed beneath the Qo surface (~ 2-3 m deep), seen in radargrams from drier periods (22-PW and 22-PD). 22-PT collected along transect C-C', reveals a deeper reflector (1.5 m) near the SEL Eddy flux tower, 0.5 m deeper than the bottom of the caliche. This reflector has not been correlated with other GPR transects or soil pit observations. The 22-PT radargram roughly coincides with soil pit observations (Figure 9). However, the processed radargram from 22-PD agrees well with depths to the top and bottom of the shallowest caliche layer below the JI surface, as seen in Figure 6-9. A deeper reflector below the Qo surface was also observed (~ 1 m depth). Caliche depths observed below the JI surface are consistent, while they were less consistent below the Qo surface, where shallow caliche is not present. Caliche is generally not present at shallow depths below the Qo surface, though fine caliche was observed in two auger holes at depths of approximately 0.8 m and 1.6 m. Drilling with a solid stem auger encountered impenetrable material ~3 m depth at two locations below the Qo surface, suggesting that in some locations, caliche may be forming or present at depth (Figures 6-8). Field observations and GPR observations for caliche boundaries have been summarized in Table 3.

Table 3: Summarizes caliche layer depths observed at out study sites.

Table 3			
Site	Estimated depth to top and bottom of shallowest caliche layer from GPR	Estimated depth to top and bottom of shallowest caliche layer from augering observations	Estimated depth to top and bottom of shallowest caliche layer from soil pit observations
JI Surface	0.3-0.6 m to 1-1.5 m	0.3-0.5 m to 1 m	0.3 m to 1m
Qo Surface	~ 2 m	1.6 m	
Playa Surface	No caliche layer	No caliche layer	No caliche layer

GPR data collected at the Playa site showed no evidence of a caliche layer but gives insight to the different mineralogy and textures beneath the Red Lake Playa (Table 4). Although there is difficulty in hand augering through gypsum-rich soils, gypsum was encountered at depths of ~30 cm using a solid stem auger attached to drill rig to describe soils beneath the playa surface. Field and GPR observations of caliche layer boundaries have been summarized in Table 3; gypsum content increases with depth, with wet soil found at approximately 2 m depth. Field observations at the playa site have been summarized in table 4, and GPR results correlate well with some changes in mineralogy and texture seen in the field.

Table 4: Summary of Playa field observations of soil

Table 4: Playa hand augering observations	
Field Observations/Depths	GPR reflections depths
0-30 cm loose sand and clay	0-30 cm
30-180 cm indurated clay with gypsum lenses	30-120 cm
180-200 cm lighter, massive white gypsum	120-180 cm
>200 cm gypsum and clay- wet to the touch- green	Not imaged

Slice view projections of the GRP radargrams, where integrated GPR reflections in 0.1 m vertical intervals along GPR transects are plotted, appear useful for identifying infiltration patterns and locate channels with exposed caliche. As seen in Figure 10, there were stronger reflections at the surface (upper 10 cm) in the 21-PW slice (wetter), when compared to the 21-PD slice (drier). Moderate reflections (indicated by light blue color) were encountered in ephemeral channels (Figure 10 and 11). Strong reflections beneath these channels disappear at about 60 cm depths. Slice view analyzed beneath the Qo surface shows a decrease in reflections after the 30 cm depth slice. There are also some areas beneath the Qo surface that exhibit stronger reflections at depth as seen in Figure 11.

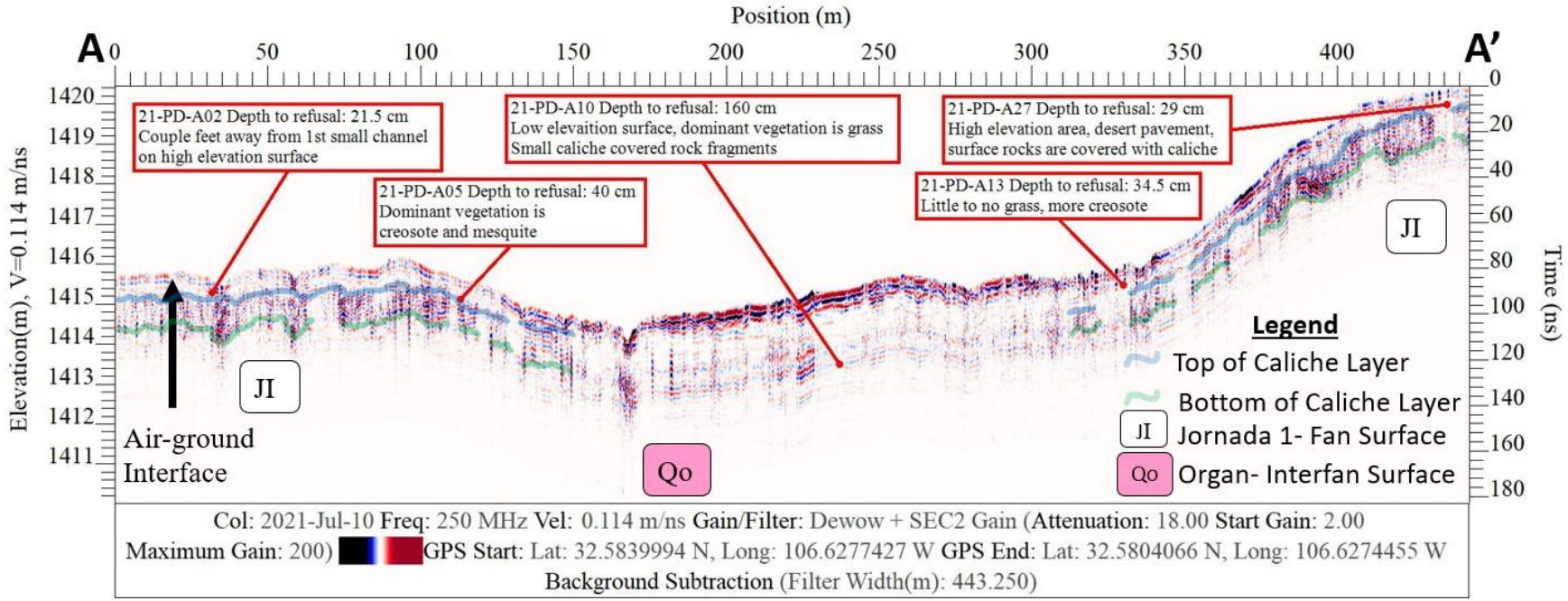

Figure 6: GPR radargram for measurement 21-PW along A-A', collected at the piedmont site on July 10, 2021. This is considered the wettest scenario.

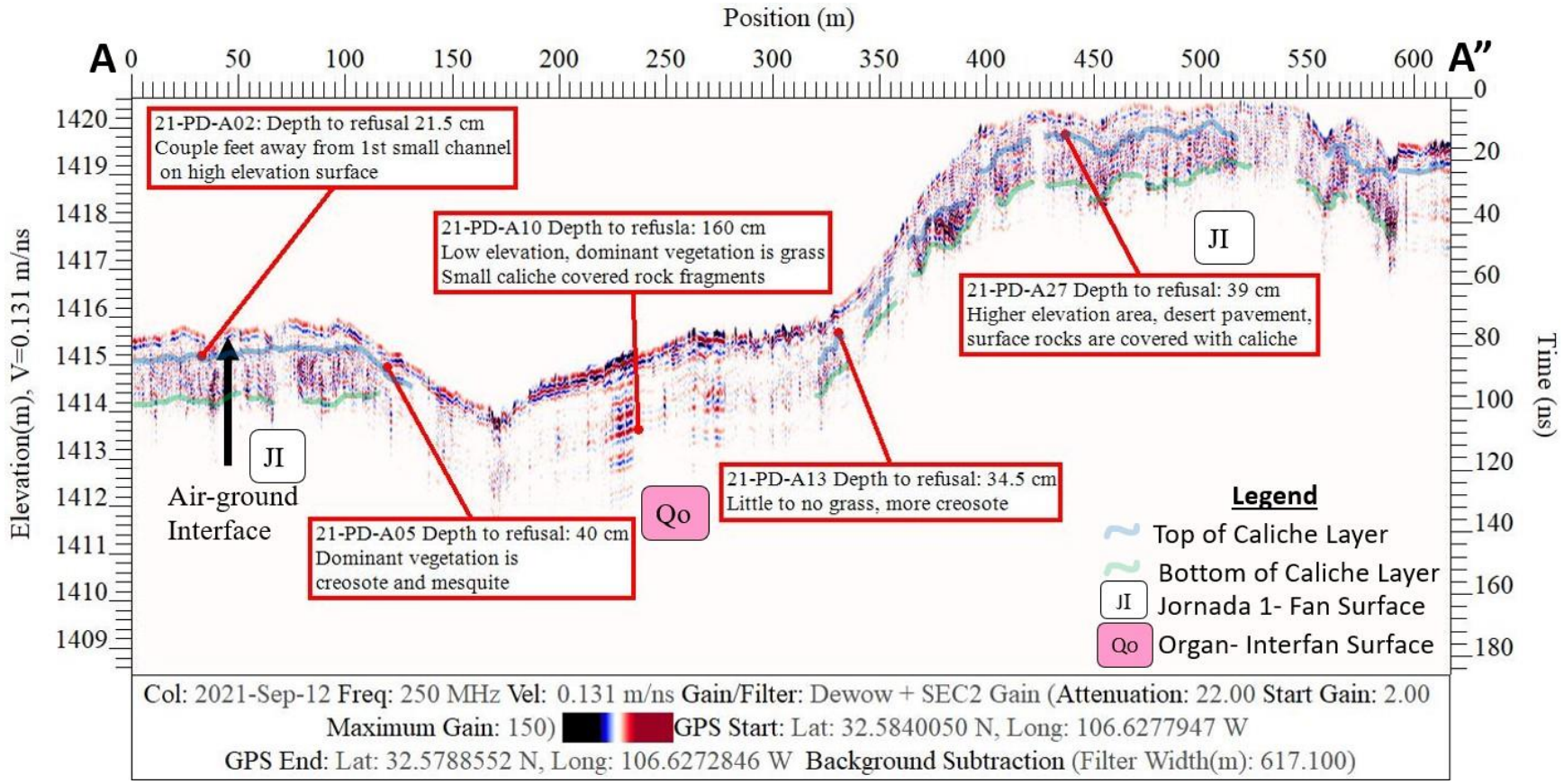

Figure 7: GPR radargram for measurement 21-PD along A-A", collected at the piedmont site on September 12, 2021. This is considered the driest scenario.

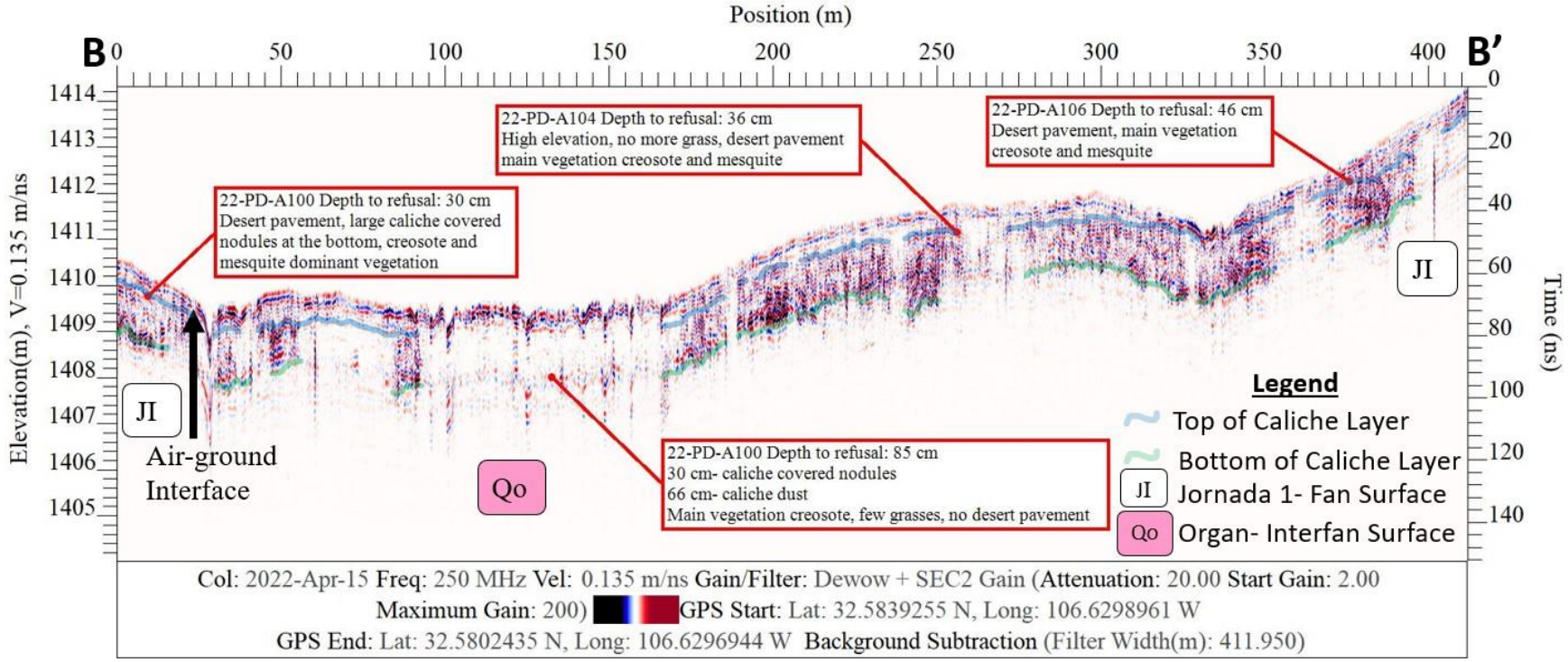

Figure 8: GPR radargram for measurement 22-PW along B-B', collected at the piedmont site on April 15, 2022. This is considered the driest scenario.

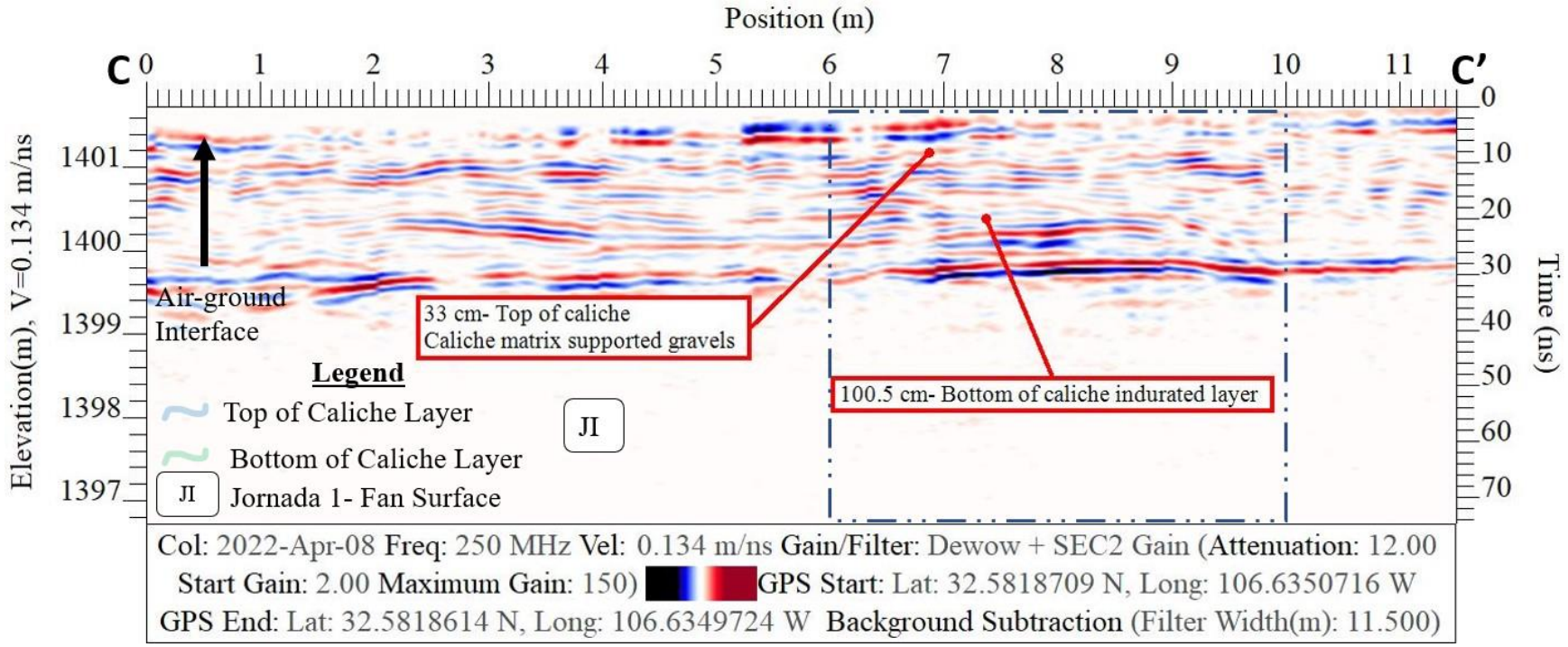

Figure 9: GPR radargram for measurement 22-PT along C-C', collected at the piedmont site on April 08, 2022.

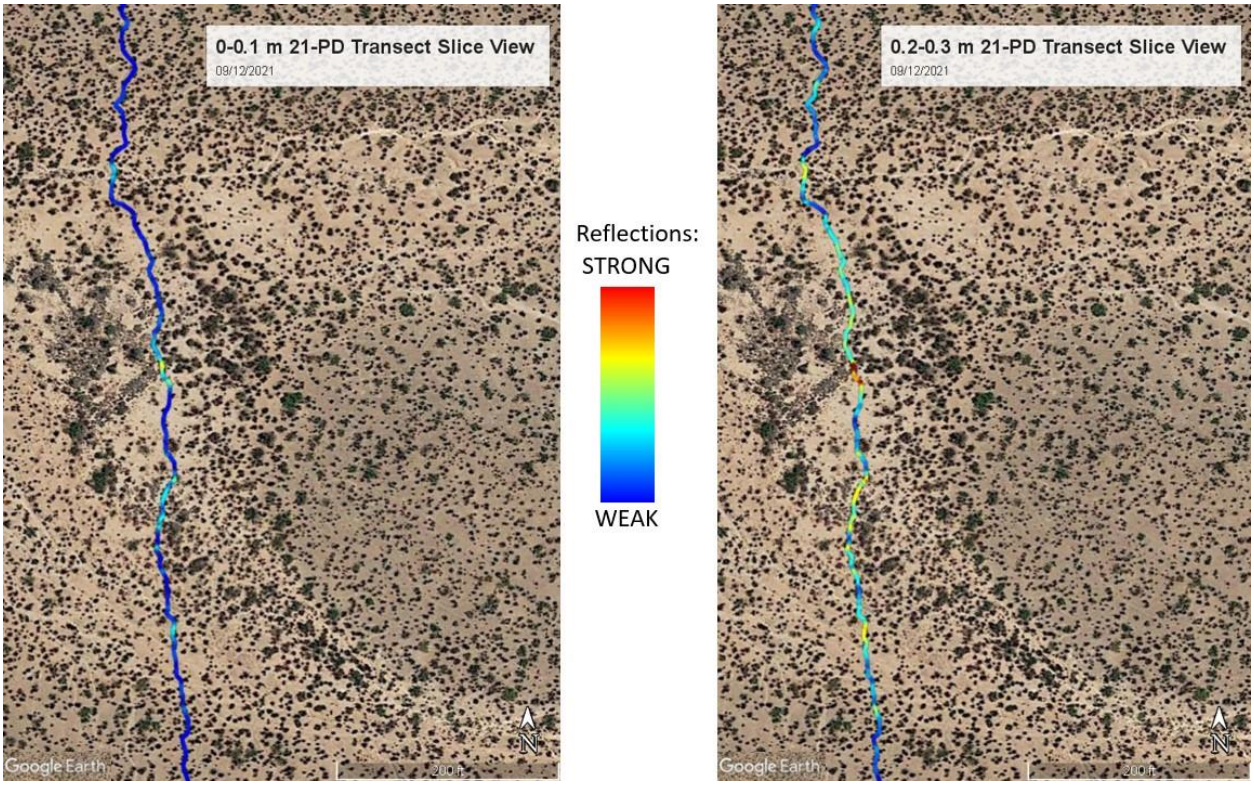

Figure 10: Slice view of comparison of 0-0.1 m depths of 21-PW and 21-PD transect.

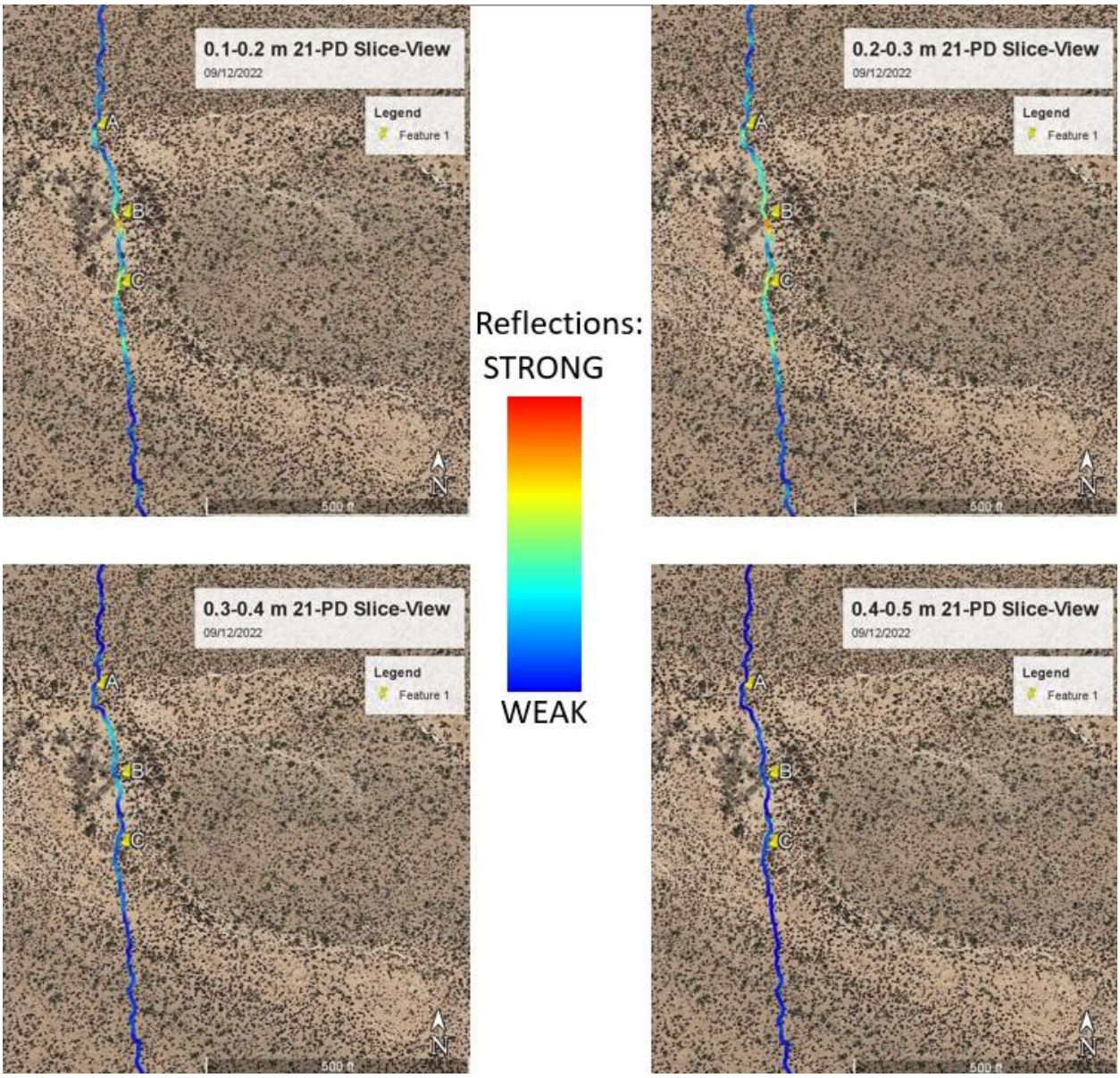

Figure 11: Slice view of comparison of 0.1-0.2 m (top left) and 0.2-0.3 (top right) m, 0.3-0.4 m (bottom left), and 0.4-0.5 m (bottom right) depths of 21-PD transect collected on 09/12/2021.

4.3 Physical Stability

This section describes the results for each term of the RUSLE implementation utilized here.

4.3.1 Rainfall erosivity (R)

The mean annual precipitation was 156 mm, and the Fournier index was 32 at the piedmont site at Jornada for 2020. Therefore Eqns. 5b and 6b are appropriate to calculate rainfall erosivity. Data from 2020 was used since they offer a complete annual record of precipitation data at Jornada, and was a moderately active monsoonal season. The values calculated for R were applied to all sites, since the sites are relatively close to one another. Rainfall erosivity factors were calculated as 164 and 45 (MJ mm ha^{-1} h^{-1} yr^{-1}) from the two equations. When converted to U.S. customary units (hundreds of foot ton-force inch $acre^{-1}$ h^{-1} $year^{-1}$), rainfall erosivity was calculated as 9.65 and 2.64 by the two different equations, respectively.

4.3.2 Soil Erodibility (K)

The M factor in this equation was calculated from soil texture data at each site, a summary of m factor calculated for each site can be seen on Table 5. The near surface soil below the JI surface has been classified as loam or clay loam (Figure 3), though field observations indicate there is a high percentage of desert pavement covering the surface. Near surface soil below the Qo surface has been classified as clay loam and sandy loam with no desert pavement. The near surface soil below the Playa surface has been classified as clay with gypsum bearing soils beneath. Organic content at Jornada Experimental Range is approximately 1% which has been acquired by other researchers working on different aspects of the Critical Zone Project (Nyachoti et al., 2019). From these findings, values of 1 or 2 (very fine granular or fine granular) were used for the structure in the equation (b) and analysis of the texture of the soils was used to determine M (particle size

parameter). Soil permeability (c) was also acquired by analyzing soil textures and was selected to range from 2-5 (moderate, slow to moderate, slow) as seen in Table 5. K values for the JI surface range from 0.10 to 0.27 ton * acre * h * [hundreds of acre-ft * tonf * in]$^{-1}$. The K value for the Qo surface was calculated as 0.15 ton * acre * h * [hundreds of acre-ft * tonf * in] $^{-1}$ and ranged from 0.07 to 0.09 ton * acre * h * [hundreds of acre-ft * tonf * in] $^{-1}$ for the playa surface (Table 5).

Table 5 Summarized textural percentages of topsoil (0-20 cm depths) samples at the site along with the calculated K factor for RUSLE.

Table 5: Summarized soil texture percentages and K factor for topsoil samples									
Site	Sample Depth	Sand %	Clay %	Silt %	M (Particle size parameter)	a Organic Content	b Structure	c Permeability	K factor
JI	19.2	27.9	37.89	34.21	2124.83	1	2	2	0.11847
JI	12	37.87	28.47	33.66	2407.87	1	2	2	0.140452
JI	15-20	25.56	0.42	32.46	1883.01	1	2	2	0.140452
JI	10	34.60	0.28	38.95	2805.55	1	2	2	0.171948
JI	20	23.98	0.24	52.45	4009.31	1	2	2	0.270877
JI	10	29.47	0.22	48.91	3833.59	1	2	2	0.25614
JI	10	44.26	0.17	39.37	3170.98	1	2	2	0.20145
JI	10	41.09	0.22	37.53	2950.85	1	2	2	0.183618
Qo	10	54.30	18.11	27.58	2258.41	1	1	4	0.146296
Playa	0	9.426	65.73	24.85	851.57	1	1	5	0.06809
Playa	0-16.5	10.46	60.42	29.12	1152.28	1	1	5	0.088915

4.3.3 Slope Length and Slope Angle (LS)

For this study, the L and S factors were combined (Wischmeier and Smith 1978). There are no irregular slopes at our site, slopes all fall within the slope range of 3 to 18%. Slope lengths used for this research are longer than what the equation has been developed for, which may introduce some error (Wischmeier and Smith 1978). At the piedmont study site, slope angle ranges from 2-3% using a slope length of 750 and 4,000 m. LS factors were calculated as 0.43 for the Qo surface and 0.76 for the JI surface.

4.3.4 Revised Universal Soil Loss Equation (A)

From inputs to RUSLE (Table 6), JI surface was calculated to have an erosivity of 1.3 ton/acre/yr while the Qo surface was calculated to have an erosivity of 0.62 ton/acre/yr. For general comparison, Pimentel et al. (1995) reported an average soil erodibility of 6.8 ton/acre/yr for croplands in the US. These numbers were converted to a vertical erosion rate (mm/yr) by applying the bulk density of the appropriate soils (JI surface = 0.2 mm/yr; Qo surface = 0.1 mm/yr). Since the depth to the top of caliche is approximately 40 cm, at a constant rate of erosion, it would take approximately 2,000 years for erosion to reach the top of the caliche and begin to erode. It is important to note the uncertainty of these calculations without in-depth parametrization should only be considered as estimates of soil erosion (Wischmeier and Smith, 1978).

Table 6 Calculated RUSLE factors for each surface, erosion potential, erosion rate, and time expected to reach the top of caliche.

Table 6: RUSLE calculations and inputs

Surface	R-Rainfall Erosivity (hundreds of foot ton-force inch $*$ $acre^{-1} * h^{-1} * yr^{-1}$)	K-Soil Erodibility (ton $*$ acre $*$ h $*$ [hundreds of acre-ft $*$ tonf $* in]^{-1}$)	LS-Slope Length & Slope Steepness (Unitless)	A-Erosion Probability (ton$*$ $acre^{-1} * yr^{-1}$)	Erosion rates (mm/yr)	Time to reach caliche top at 40 cm depth (Years)
JI	9.65	0.18	0.3	1.3	0.2	2,000
Qo	9.65	0.15	0.28	0.62	0.1	

4.4 Chemical Stability

4.4.1 Soil Moisture Analysis

At one site where caliche was not observed (at the Grassy Pit below the Qo surface), TDR soil moisture profiles show that water only penetrated the upper 0.3 m of the profile after the large rainfall event (2.5 mm of rain) in July 2021, as seen in Figure 12. The soil pit below the Qo surface exhibited an apparent 2.5% increase in soil moisture the 100 cm probe, which could be water accumulating at that depth or temperature-associated drift in TDR measurement, in response to these large monsoonal rain events (Figure 12). During the wettest measurement period (July 2021), locally elevated soil moisture was retained in the upper 10 cm while during a drier period (September 2021) it was retained at 30 cm depths at the grassy pit site located beneath the Qo surface (Figure 11 and 12). However, a lack of soluble chloride along a 3-m deep

vertical array of samples below the Qo surface suggests that there is downward flushing of soil moisture at longer time scales. As expected, there was less soil moisture during dry conditions (Figure 10). Figure 13 shows a lagged response after large rainfall events in the probe just above the caliche (32 cm) beneath the JI surface. Volumetric water content measurements for TDR profiles in the caliche have not been calibrated, but higher soil moisture was observed in this sensor during monsoon season (50 cm probe in Figure 13). Soil moisture data from the south pit also exhibited a lagged response in the probe just above the caliche (29 cm depth) beneath the JI surface (Figure 14). For the soil moisture sensor pit dug near the SEL eddy flux tower on top the JI surface at the Piedmont site, the corresponding data also exhibited a delayed response to precipitation events in the sensor just above the caliche (42.5 cm) providing evidence of soil water movement to the top of the caliche beneath the JI surface (Figure 15). The probe installed near the bottom of the caliche layer at 100.5 cm depth at SEL soil pit also exhibits higher volumetric water content like the 50 cm probe installed near the top of the caliche layer at the West pit (Figure 13 and 15). However, strong correspondence between those soil moisture changes, and soil temperature suggests these trends are attributed to temperature related variability suggesting the variations are largely a measurement artifact (Figure 16 and 17). Along the D-D' soil moisture transect, where sensors were uniformly installed at 20 cm depths (Figure 1), the water content increases about 20-30% between probes D and E in response to a rainfall event in January 2022, which are located near base of the slope on the JI surface (Figure 18). Besides probes D and E, the other probes recorded a volumetric water content of 5%, the slight increase in all probes around February 2022 appears temperature related, rather than a result from a change in soil moisture. These results suggest there is a lateral flow above the caliche from the JI surface toward the Qo surface, after large rainfall events (Figure 18). No data

indicates measurable water flux into or below the caliche, though the number of sensors in these locations are limited (n=2).

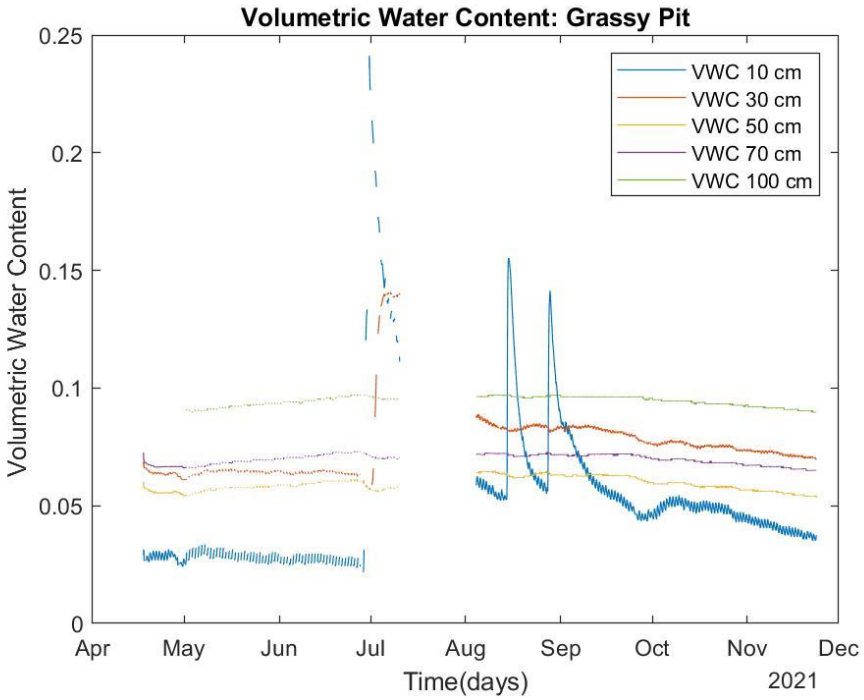

Figure 12: Volumetric water content from the Grassy pit, below the Qo surface.

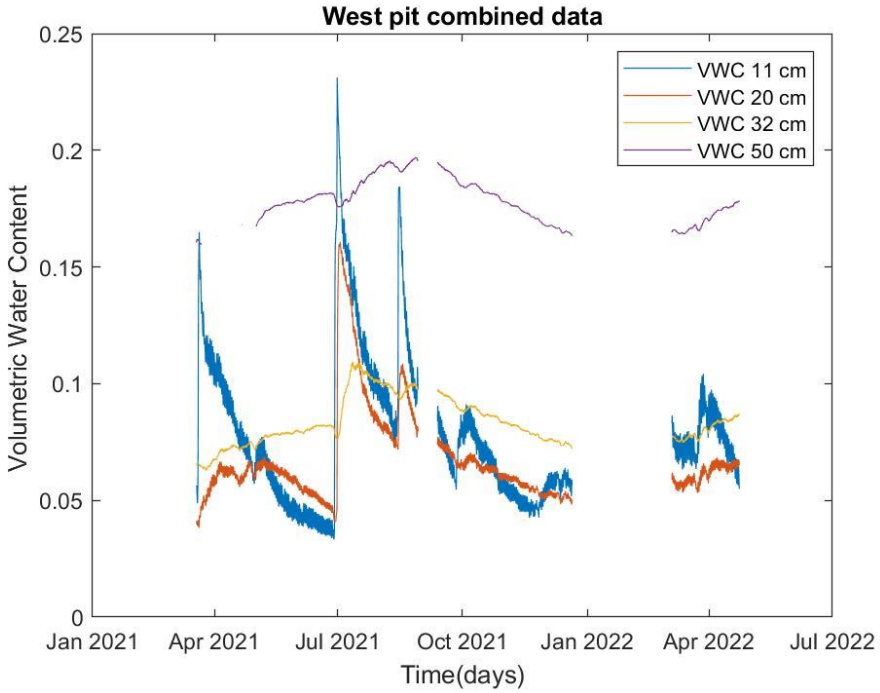

Figure 13: Volumetric water content for the West pit, below the JI surface.

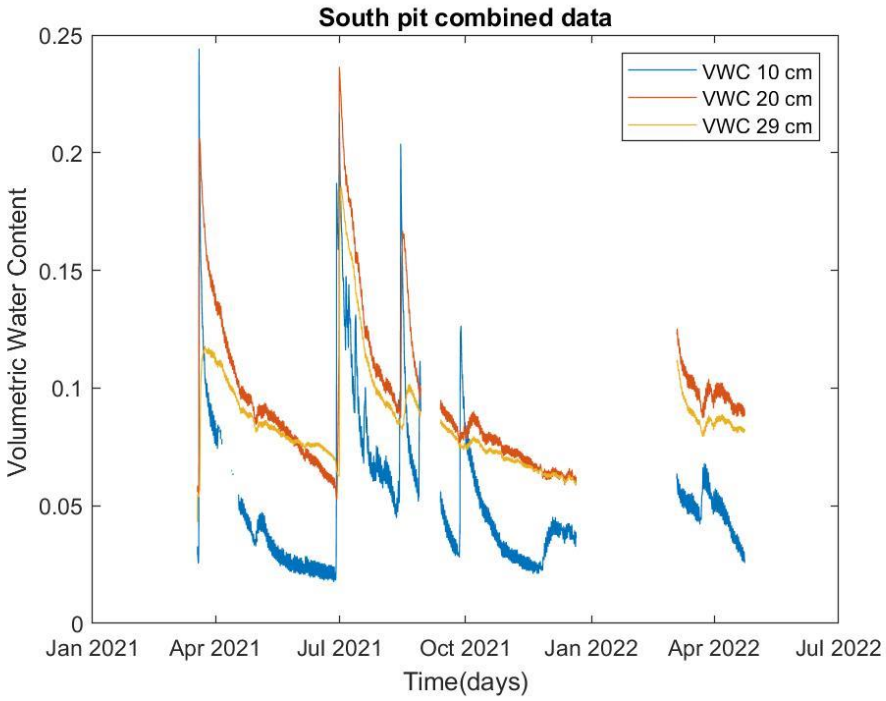

Figure 14: Volumetric water content for the South pit, below the JI surface.

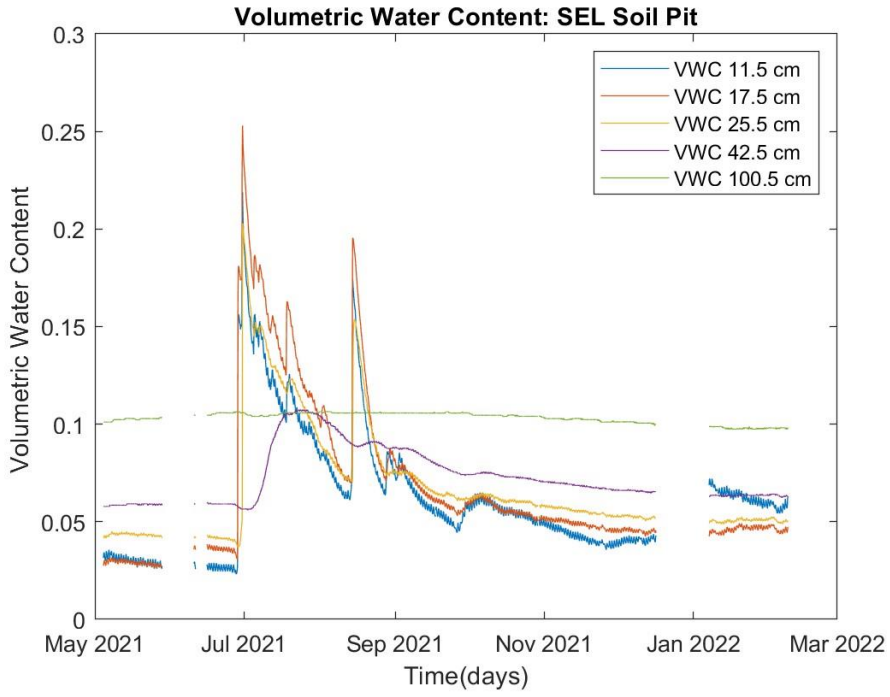

Figure 15: Volumetric water content at the SEL eddy flux tower, below the JI surface.

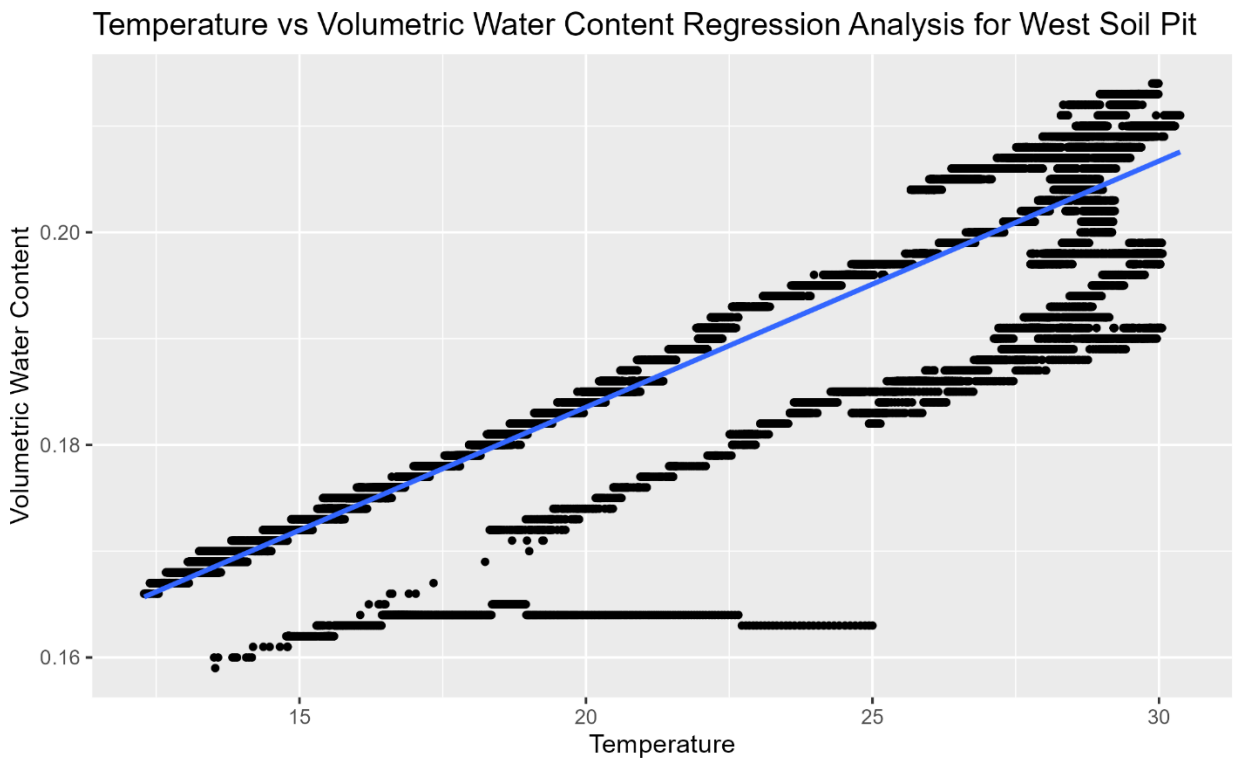

Figure 16: Regression showing high temperature dependence (R^2=0.89) for West soil pit.

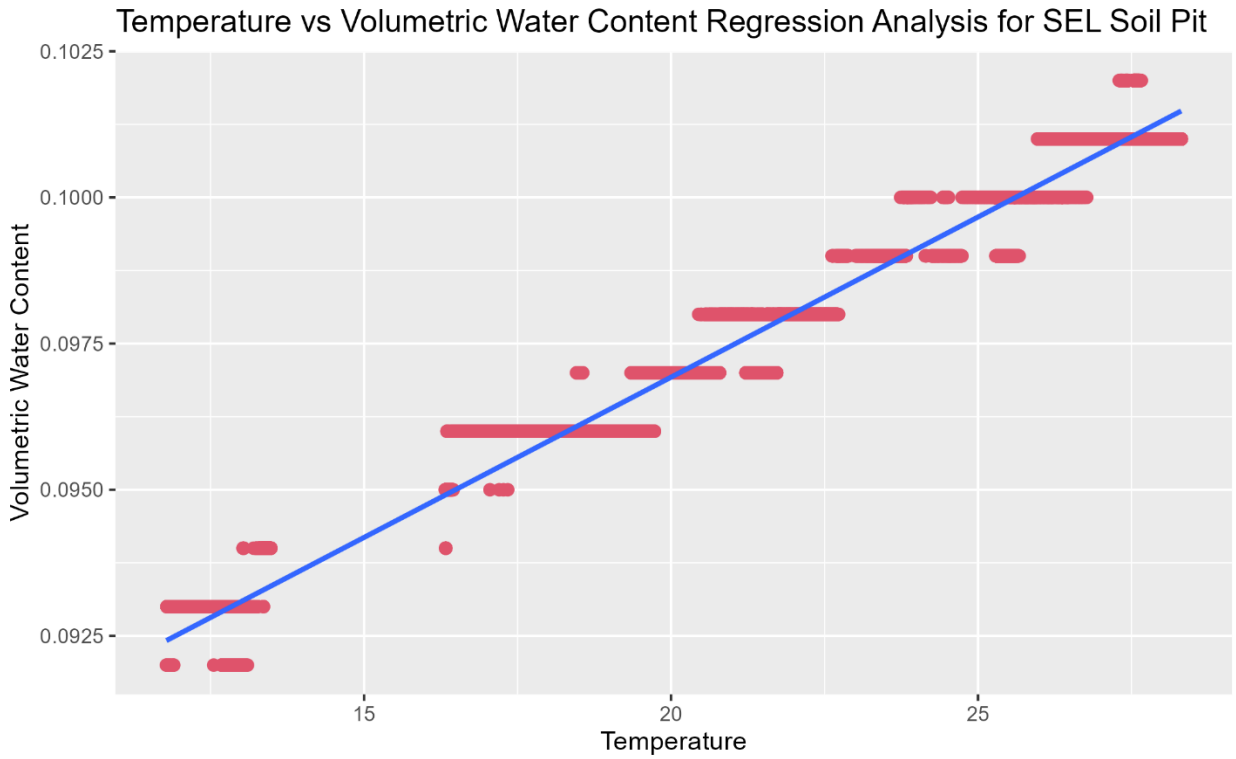

Figure 17: Regression showing high temperature dependence (R^2=0.98) for SEL soil pit.

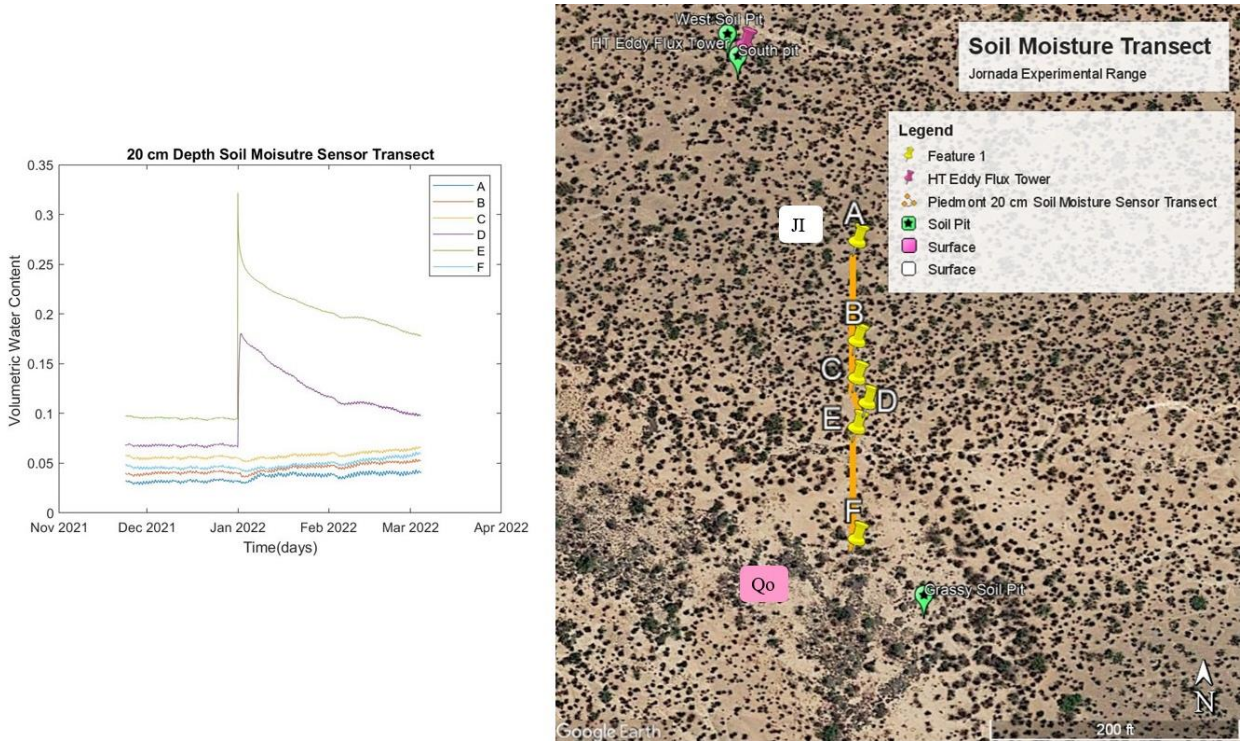

Figure 18: Volumetric water content for the soil moisture probes in transects installed beneath the JI surface along with map showing location of sensors installed at a 20 cm depth.

Section 5: Discussion

Results from this research suggest that GPR is a useful tool for delineating surfaces of shallow, well-developed caliche layers in desert soils. The ability of GPR to map caliche was slightly impacted by seasonal variations between wettest to drier periods (July 2021, September 2021, and April 2022). That is, GPR data collected during the wetter and drier periods were both successful in identifying shallow caliche boundaries, with little to no variations in their interpreted depths between the runs and auger observations though velocity calculations had to be modified for each season based on in situ permittivity values from local TDR probes. For example, GPR measurement 22-PD, collected along B-B' transect (200 m west from A-A'/A" transects) coincides with the observed caliche patterns on all the other transects collected on other dates. Top boundaries of the shallowest caliche layers (0.3-0.5 m deep) interpreted from processed 21-PW and 21-PD GPR radargrams agreed with field observations of their depths from hand augering and soil pit observations. The observed bottom of the shallowest caliche layer can also be seen in 21-PW and 21-PD (0.8-1.2), soil moisture sensor pit observations coincided with the bottom of the caliche observed in 22-PT collected near the SEL Eddy covariance tower (1 m depth) indicating that interpretations of the bottom and top of caliche layer were being properly imaged and interpreted. The JI older alluvial fan surface which exhibits lower erosion (based on RUSLE calculations) and a dense desert pavement layer in underlain by shallow (0.3-0.5 cm) stage IV caliche. While the topographically lower Qo surface does not appear to be underlain by competent, shallow caliche layers, there is some evidence of older caliche layers/remnants at depths of 2-3 m. Stronger air-ground reflections along Qo surface were observed during the wet period relative to dry periods because of stronger near-surface reflections caused by the high soil moisture at shallow depths, which limited deeper

imaging. Past research has noted the advantages of collecting seasonal GPR because water (dielectric permittivity of 80) greatly increases the dielectric permittivity of soils (Zhang et al., 2014) which can modify the ability of GPR to identify certain types of material interfaces. However, few seasonal GPR variations were observed at our specified sites between measurement taken from a wet period (July 2021) vs. a dry period (September 2021). The minimal variations in GPR response between wetter vs. drier periods found during this research could be due to the presence of caliche or limited soil saturation that would have otherwise created greater reflections between the two runs. That is, if only marginal increases in soil water saturation occur, then permittivity of the soil above the caliche would not increase markedly, making the reflection relatively similar between wetter vs. drier periods. The reflector below Qo observed during dry conditions may be due to evapotranspiration from shallow grass roots supported by soil moisture observations. The caliche boundaries interpreted from the 22-PT radargram were roughly coincident with soil pit observations possibly because the boundaries observed in the soil pit are gradual (Figure 9).

Slice view profiles of the GPR data appear useful for tracking the depth of infiltration after precipitation events, by analyzing changes in the strength of a reflection through 10 cm slices of the GPR radargram (Figure 10 and 11). At wetting front boundaries, where sharp contrasts in soil moisture exist, slice view produces strong reflections in the corresponding depth of the wetting front due to the significant impacts on the reflection coefficients along wetting fronts (Eq. 1). The slice view of the first 10 cm of 21-PD and 21-PW appears to be mapping reflections at the boundary of soil wetting during the wettest period (21-PW; Figure 6). Similarly, the infiltration depth seen in soil moisture arrays coincided with the decreased reflections seen at 30 cm depths on slice view, suggesting the slice view imaging of radargrams

in dryland environments allows for 2-D extrapolation of soil moisture wetting fronts (Figures 11 and 12). We interpret the increased reflections near channels as a result from higher permittivity of the caliche relative to air than the adjacent porous soil (larger air-ground interface reflection; Figures 10 and 11). The depth of which the strong reflections beneath caliche disappear could possibly mark the bottom boundary of caliche in channels. While our findings indicate GPR was a viable tool to investigate the extent of caliche, other tools were needed to further investigate caliche stability via examination of physical erosion and soil water flux/distribution.

Erosion can affect caliche stability by removing calcium sources necessary for caliche formation or by removing the exposed caliche itself. Erosion rates can hence be used as a marker for land degradation as well as caliche stability. Erosion rates calculated from RUSLE at the piedmont site at JER are higher on the JI surface than on the Qo surface, but they are still considered relatively low when compared to other studies conducted in a watershed (Chandramohan et al., 2002). However, due to the natural nature of each factor there are high errors associated with RUSLE equations and hence should just be taken as an approximation (Benavidez et al., 2018; Ghosal and Das Bhattacharya, 2020). The JI surface is covered by desert pavement, which is not considered in RUSLE estimates and is known to reduce surface erosion rates considerably (Matmon et al., 2009). Thus, the relatively low erosion rates calculated for both surfaces indicate that they are physically stable, as defined here. Using estimated erosion rates, caliche below these surfaces may be exposed in several thousand years, but the dense desert pavement seen on the JI surface would slow down this process considerably. In the case that caliche is exposed at the surface, such as in present-day channels, caliche would lead to carbonate dissolution and decrease erosion rates at the surface (Zamanian et al., 2016). Dissolution can limit caliche formation or produce caliche reprecipitation in deeper intervals.

Similarly, thinning of caliche because of increased dissolution caused by channeled runoff was suggested by Wilson et al. (2005). They also noted sites where caliche had possibly been eroded or dissolved occur at topographic lows (Wilson et al., 2005). Caliche is also expected continue forming into a thicker layer below JI surfaces, barring limiting controls in response to climate change.

Climate is one of the most important factors that controls caliche development, due to precipitation and temperature leading to the leaching, evaporation, and re-precipitation that is essential for caliche formation (Zamanian et al., 2016). The amount of precipitation at Jornada (250 mm/yr) has been shown to produce the desired scenario to form shallow caliche layers (Zamanian et al., 2016). Precipitation levels above 500 mm/yr would likely lead to too much soil moisture or vertical water flux for caliche to be able to form at shallow depths (Zamanian et al., 2016). The patterns seen in soil moisture distribution also greatly influence the depth and possibility of caliche formation due to the continued water fluxes necessary for caliche formation. The soil water distribution seen after large rainfalls at Jornada indicates the possibility of forming thicker caliche layers beneath the JI surface if calcium sources continue arriving from dust. Since the depth of infiltration coincides with the caliche top beneath the JI surface, caliche formation is facilitated if limited infiltration occurs due to the already present calcium sources. Too much infiltration may limit continued precipitation and evaporation of calcium sources needed to form caliche. Hence, there is a fine balance between the amount of precipitation/infiltration needed to create conditions favoring caliche formation/growth. Soil moisture below the Qo surface was expected to have higher soil moisture since it is in a topographically low site, but the infiltration analyzed for 2021 shows infiltration was limited to the upper 30 cm during monsoon season. Additional supporting data for water-soluble chloride

concentrations from soil samples from a ~3m hole near the Grassy Pit site reveals that deep water infiltration does appear to have occurred at the site. If chloride has been flushed through the soil by water, it is likely that calcium sources may not be accumulating at shallow depths on the Qo surface. A conceptual model which includes significant flushing of water through the soil also does not support continued precipitation/evaporation necessary for caliche development to later stages. The fact that there is fine caliche and few caliche covered nodules beneath the Qo surface could mean there are early stages of caliche beneath this surface or older caliche horizons at depth. In terms of caliche stability, due to the low water flux and generally low soil moisture seen at the JI site, we have classified it as a chemically stable surface. Our data from 2020 and 2021 also suggest that the material below the Qo surface may produce conditions where caliche is chemically stable, but the longer-term chloride data indicate that conditions for shallow (<1m) caliche development are not supported on longer time scales and that caliche is not chemically stable at the location.

There are external factors that influence the observed results and interpretations like the caliche formation rates, and uncertainties and limitations with our data. These errors include both approximation of the RUSLE factors and the empirical nature of the model itself. The associated errors with RUSLE can become even higher since it has been used in a non-agricultural setting in this study unlike the agricultural conditions that the RUSLE has been developed for (Wischmeier and Smith 1978). A detailed meteorological record is necessary to correctly estimate rainfall erosivity (R) factor, due to seasonal variations that may not be captured using a one-year record like this study. Since the JI surface is covered by a dense desert pavement layer, the calculated soil erodibility would be negatively impacted if it were possible to account in RUSLE calculations. Our classifications largely depend on the controlling factors of physical and

chemical caliche stability to remain relatively the same, since caliche forms over thousands of years. The observed factors may be severely impacted by increased aridity expected because of climate change, if so, it would be necessary to calculate new approximations to account for this change. Increasing the temporal scale of the study would decrease many uncertainties within the research.

Section 6: Conclusion

Findings from this study include:

1) GPR (250 MHz) was effective at delineating shallowest stage V caliche layer (0.3-0.5 m depth to top and 1-1.5 m depth to bottom, where present) under a range of climatic conditions. Seasonal variations in the ability to delineate these layers were relatively minor.
2) GPR slice view plots combined with soil moisture arrays at variable depths after precipitation events allow for 2-D mapping of the depth of penetration of the wetting front across multiple geomorphic surfaces.
3) Initial results support our hypothesis that caliche is present in sites of surface stability and low water flux and/or soil moisture content. Our investigations of erosion potential and water distribution at Jornada Experimental suggest that the JI surface is both physically and chemically stable, the Qo surface is physically but not chemically stable, and the Red Lake playa is possibly non physically or chemically stable (Figure 19).

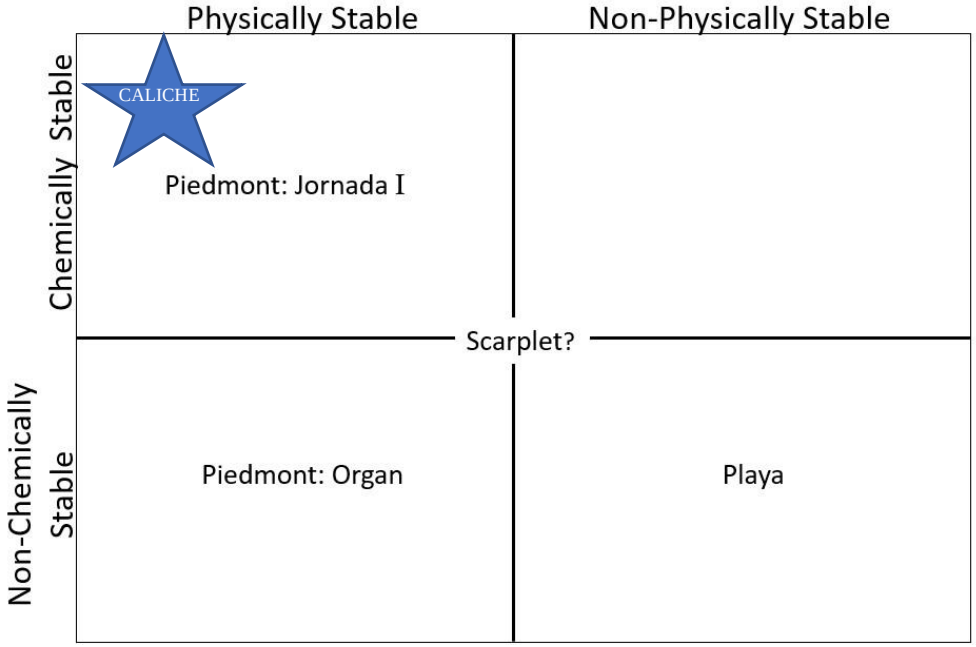

Figure 19: Updated chemical and physical caliche stability matrix reflecting findings.

Future work to support these findings includes analyzing caliche stability of different surfaces and using additional physical and chemical caliche stability markers. The limitations encountered during this research can be reduced with follow-up work. Now that surfaces have been categorized by their caliche stability, analyzing additional surfaces around Jornada Experimental Range can aid in fully understanding caliche stability at this site. Additional surfaces could include alluvial flat and scarplet sites found around Jornada. The additional sites would also aid in creating a comprehensive map of caliche in its different stages and caliche layer boundaries found at Jornada Experimental Range. Physical and chemical caliche stability markers used here were erosion by water and soil moisture distribution, respectively. To fully understand caliche stability additional physical and chemical markers like chloride mass balance data, erosion by wind, and biocrust analysis could supplement the findings. Since we suspect there are older caliche layers beneath the Qo surface, drilling through the different layers in this surface can shed light to the deeper reflections seen in our GPR results. The soil moisture movement observed on top of caliche layers and associated dissolution rates would further investigate caliche stability beneath the JI surface.

References

Archer, S. R., & Predick, K. I. (2008). *Climate Change and Ecosystems of the Southwestern United States*. *Society of Range Management*, 7.

Benavidez, R., Jackson, B., Maxwell, D., & Norton, K. (2018). A review of the (Revised) Universal Soil Loss Equation ((R)USLE): With a view to increasing its global applicability and improving soil loss estimates. *Hydrology and Earth System Sciences*, *22*(11), 6059–6086. https://doi.org/10.5194/hess-22-6059-2018

Buffington, L. C., & Herbel, C. H. (1965). Vegetational Changes on a Semidesert Grassland Range from 1858 to 1963. *Ecological Monographs*, *35*(2), 139–164. https://doi.org/10.2307/1948415

Canup, T. (2000). A Pilgrimage to the Desert Project. *NMSU College of Argicultural, Consumer, and Environmental Sciences, New Mexico Resources*, 71–74.

Chandramohan, T., & Durbude, D. G. (2002). Estimation of soil erosion potential using Universal Soil Loss Equation. *Journal of the Indian Society of Remote Sensing*, *30*(4), 181–190. https://doi.org/10.1007/BF03000361

Craig Tweedie (2021), AmeriFlux BASE US-Jo1 Jornada Experimental Range Bajada Site, Ver. 1-5, AmeriFlux AMP, (Dataset). https://doi.org/10.17190/AMF/1767833

Curtis Monger, H. (2006). Soil Development in the Jornada Basin. In H. Curtis Monger, *Structure and Function of a Chihuahuan Desert Ecosystem*. Oxford University Press. https://doi.org/10.1093/oso/9780195117769.003.0008

Duniway, M. C., Herrick, J. E., & Monger, H. C. (2007). The High Water-Holding Capacity of Petrocalcic Horizons. *Soil Science Society of America Journal*, *71*(3), 812–819. https://doi.org/10.2136/sssaj2006.0267

Duniway, M. C., Herrick, J. E., & Monger, H. C. (2010). Spatial and temporal variability of plant-available water in calcium carbonate-cemented soils and consequences for arid ecosystem resilience. *Oecologia*, *163*(1), 215–226. https://doi.org/10.1007/s00442-009-1530-7

Durner, W., & Iden, S. C. (2021). The improved integral suspension pressure method (ISP+) for precise particle size analysis of soil and sedimentary materials. *Soil and Tillage Research*, *213*, 105086. https://doi.org/10.1016/j.still.2021.105086

Durner, W., Iden, S. C., & von Unold, G. (2017). The integral suspension pressure method (ISP) for precise particle-size analysis by gravitational sedimentation: ISP METHOD FOR PARTICLE-SIZE ANALYSIS. *Water Resources Research*, *53*(1), 33–48. https://doi.org/10.1002/2016WR019830

Ghosal, K., & Das Bhattacharya, S. (2020). A Review of RUSLE Model. *Journal of the Indian Society of Remote Sensing*, *48*(4), 689–707. https://doi.org/10.1007/s12524-019-01097-0

Gibbens, R. P., & Beck, R. F. (1988). Changes in Grass Basal Area and Forb Densities over a 64-Year Period on Grassland Types of the Jornada Experimental Range. *Journal of Range Management*, *41*(3), 186. https://doi.org/10.2307/3899165

Gile, L. H., Grossman, R. B., & Service, U. S. S. C. (1979). *The Desert Project Soil Monograph: Soils and Landscapes of a Desert Region Astride the Rio Grande Valley Near Las Cruces, New Mexico*. U.S. Department of Agriculture, Soil Conservation Service. https://books.google.com/books?id=CTfdy68YHMgC

Gile, L. H. (1999). Eolian and Associated Pedogenic Features of the Jornada Basin Floor, Southern New Mexico. *Soil Science Society of America Journal*, *63*(1), 151–163. https://doi.org/10.2136/sssaj1999.03615995006300010022x

Havstad, K. M., Huenneke, L. F., & Schlesinger, W. H. (2006). *Structure and Function of a Chihuahuan Desert Ecosystem: The Jornada Basin Long-Term Ecological Research Site*. Oxford University Press. https://books.google.com/books?id=-T8PpZ5Xn4wC

Hennessy, J. T., Gibbens, R. P., Tromble, J. M., & Cardenas, M. (1983). Water Properties of Caliche. *Journal of Range Management*, *36*(6), 723. https://doi.org/10.2307/3898195

Li, J., Okin, G. S., Alvarez, L., & Epstein, H. (2007). Quantitative effects of vegetation cover on wind erosion and soil nutrient loss in a desert grassland of southern New Mexico, USA. *Biogeochemistry*, *85*(3), 317–332. https://doi.org/10.1007/s10533-007-9142-y

Mack, G. H., McIntosh, W. C., Leeder, M. R., & Curtis Monger, H. (1996). Plio-pleistocene pumice floods in the ancestral Rio Grande, southern Rio Grande rift, USA. *Sedimentary Geology*, *103*(1–2), 1–8. https://doi.org/10.1016/0037-0738(96)00009-7

Matmon, A., Simhai, O., Amit, R., Haviv, I., Porat, N., McDonald, E., Benedetti, L., & Finkel, R. (2009). Desert pavement-coated surfaces in extreme deserts present the longest-lived landforms on Earth. *Geological Society of America Bulletin*, *121*(5–6), 688–697. https://doi.org/10.1130/B26422.1

Monger, H. C., Gile, L. H., Hawley, J. W., & Grossman, R. B. (2009). The Desert Project—An Analysis of Aridland Soil-Geomorphic Processes. *New Mexico State University*, 77.

Neal, A. (2004). Ground-penetrating radar and its use in sedimentology: Principles, problems and progress. *Earth-Science Reviews*, *66*(3–4), 261–330. https://doi.org/10.1016/j.earscirev.2004.01.004

Nyachoti, S., Jin, L., Tweedie, C. E., & Ma, L. (2019). Insight into factors controlling formation rates of pedogenic carbonates: A combined geochemical and isotopic approach in dryland

soils of the US Southwest. *Chemical Geology*, *527*, 118503. https://doi.org/10.1016/j.chemgeo.2017.10.014

Rango, A., Snyder, K., Herrick, J., Havstad, K., Gibbens, R., Wainwright, J., & Parsons, T. (n.d.). *Historical and Current Hydrological Research at the USDA/ARS Jornada Experimental Range in Southern New Mexico*. 7.

Renard, K. G., & Freimund, J. R. (1994). Using monthly precipitation data to estimate the R-factor in the revised USLE. *Journal of Hydrology*, 23.

Reuter, S., Cadol, D., Phillips, F. M., & Newton, B. T. (2021). Evaluating Focused Aquifer Recharge in the Jornada Experimental Range, NM, using Chloride Profile Analysis. *New Mexico Water Resources Research Institute*, 43.

Takahashi, K., Igel, J., Preetz, H., & Sato, M. (2015). Sensitivity analysis of soil heterogeneity for ground-penetrating radar measurements by means of a simple modeling: Sensitivity Analysis of Soil for GPR. *Radio Science*, *50*(2), 79–86. https://doi.org/10.1002/2014RS005499

Topp, G. C., Davis, J. L., & Annan, A. P. (1980). Electromagnetic determination of soil water content: Measurements in coaxial transmission lines. *Water Resources Research*, *16*(3), 574–582. https://doi.org/10.1029/WR016i003p00574

Wilson, T. H., Wells, A. W., Diehl, J. R., Bromhal, G. S., Smith, D. H., Carpenter, W., & White, C. (2005). Ground-penetrating radar survey and tracer observations at the West Pearl Queen carbon sequestration pilot site, New Mexico. *The Leading Edge*, *24*(7), 718–722. https://doi.org/10.1190/1.1993266

Wischmeier, W. H., & Smith, D. D. (1978). *Predicting Rainfall Erosion Losses: A Guide to Conservation Planning* (Vol. 537). United States Department of Agriculture.

Young, R. A., & Sun, J. (1999). Revealing stratigraphy in ground-penetrating radar data using domain filtering. *GEOPHYSICS*, *64*(2), 435–442. https://doi.org/10.1190/1.1444548

Zajícová, K., & Chuman, T. (2019). Application of ground penetrating radar methods in soil studies: A review. *Geoderma*, *343*, 116–129. https://doi.org/10.1016/j.geoderma.2019.02.024

Zamanian, K., Pustovoytov, K., & Kuzyakov, Y. (2016). Pedogenic carbonates: Forms and formation processes. *Earth-Science Reviews*, *157*, 1–17. https://doi.org/10.1016/j.earscirev.2016.03.003

Zhang, J., Lin, H., & Doolittle, J. (2014). Soil layering and preferential flow impacts on seasonal changes of GPR signals in two contrasting soils. *Geoderma*, *213*, 560–569. https://doi.org/10.1016/j.geoderma.2013.08.035

Vita

Nohemi Valenzuela Garay was born in Cuidad Juarez, Chihuahua to Norma Aracely Valenzuela Garay and Carlos Valenzuela. Her parents decided to move to El Paso, Texas, when she was three years old, where she was raised. Nohemi attended Mission Early College High School where she graduated with her Associate of Arts degree from the El Paso Community College a semester early on Fall 2015 and went on to graduate from high school on Spring 2016. After graduating with her Associate of Arts degree, she was accepted to the University of Texas at El Paso where she started her Bachelor degree of Science in Geological Sciences in Spring 2016. During her last semester as an undergraduate Nohemi participated in undergraduate research with Dr. Diane I. Doser; she focused on web-based research conducted using excel spreadsheets and graphs to correlate changes in the groundwater quality with the known human activity, and geology in the Mesilla Basin. In Fall 2020 she graduated with a Bachelor degree of Science in Geological Sciences from the University of Texas at El Paso with cum laude honors and received the award for Outstanding Undergraduate student in Geological Sciences. Then, Nohemi pursued a Master of Science from the University of Texas at El Paso on Spring 2021 with Dr. Mark Engle as her mentor. Nohemi worked as a Research Assistant with the Dryland Critical Zone Project and a Teaching Assistant during her graduate studies. In December 2022, Nohemi graduated with a Master of Science from the University of Texas at El Paso and was awarded Outstanding Graduate Student in Geological Sciences.